Applied Geochemistry 121 (2020) 104712

Contents lists available at ScienceDirect

Applied Geochemistry

journal homepage: http://www.elsevier.com/locate/apgeochem

Transfer processes of potential toxic elements (PTE) between rock-soil systems and soil risk evaluation in the Baoshan area, Yunnan Province, Southwest China

Li Zhang [a,b,c], Jennifer McKinley [d], Mark Cooper [e], Wei Han [a,c], Fei Liu [a,c], Yuntao Song [a,c], Min Peng [a,b,c], Xiujin Liu [a,c], Wei Yang [f], Hangxin Cheng [a,c,*]

[a] Key Laboratory of Geochemical Cycling of Carbon and Mercury in the Earth's Critical Zone, Institute of Geophysical & Geochemical Exploration, Chinese Academy of Geological Sciences, Langfang, 065000, China
[b] China University of Geosciences, Beijing, 100083, China
[c] Research Center of Geochemical Survey and Assessment on Land Quality, China Geological Survey, Langfang, 065000, China
[d] School of Natural and Built Environment, Queen's University Belfast, Belfast, BT7 1NN, UK
[e] Geological Survey of Northern Ireland, Belfast, BT4 3SB, UK
[f] Hubei Geological Research Laboratory, Wuhan, 430034, China

ARTICLE INFO

Editorial handling by Prof. M. Kersten

Keywords:
Potential toxic elements (PTE)
Rock-soil systems
Geochemical fluxes
Compositional data analysis (CoDA)
Geo-accumulation index (I_{geo})
Enrichment factor (EF)
Southwest China

ABSTRACT

Geochemical fluxes in rock-soil systems are important tools in the evaluation of soil environmental risk, especially where the geological background (parent materials) are enriched in potential toxic elements (PTE). In the Baoshan area, the presence of mineral resources along with carbonate and basalt parent materials often leads to PTE being elevated in soils. In this study, we compared rock and soil geochemical compositions by collecting rock samples from the host formations and ore samples from two mineral deposits (Cu–Pb–Zn and Fe–Cu–Pb–Zn) and their overlying soils. This research demonstrates enrichment of PTE (As, Cd, Cr, Cu, Hg, Ni, Pb and Zn) in soils relative to their parent materials. The enrichment in soils may be due to the removal of mobile elements (e.g., Ca, Na, Mg, and Sr), and coprecipitation (As, Cd, Cr, Cu, Hg, Ni, Pb and Zn) and/or adsorption by Fe-oxy-hydroxides (Cr and Ni) under the influence of high pH values during soil formation. The results point to a parent lithological origin and natural enrichment of PTE in Baoshan soils. However, anthropogenic contamination of soils near mining areas is also possible. Soils forming from carbonate rocks, basalts, and especially from mineralized formations have higher PTE concentrations, and in places, levels can exceed the risk screening values for soil contamination of agricultural land of China. Where the latter is the case, it is suggested that ecological monitoring be implemented in the study area. The conventional use of the geo-accumulation index (I_{geo}) and enrichment factor (EF) methods is challenged in this research and found to underestimate the PTE contamination. A compositional data analysis approach (using clr biplots) is presented which shows that comparison with regional-scale background datasets is essential to provide a more informative approach to evaluate the risk of soil contamination, especially in regions with elevated levels of PTE in parent materials.

1. Introduction

Soil sustains all terrestrial organisms and is the medium for all biogeochemical processes. However, it is a finite resource that is not renewable on a human time scale (Purswani and Pathak, 2018). With competing pressures between population, resources and environment, soil quality has become a major concern globally (Antibachi et al., 2012; Cheng et al., 2014a, 2014b; 2014c, 2014d; Cicchella et al., 2008; Gong et al., 2014; Li et al., 2010, 2014a; Luo et al., 2012; Zhang et al., 2013). Sources of potential toxic elements (PTE) are most often considered to be anthropogenic origin (e.g. industrial and mining activities, agricultural fertilization, and irrigation and urban living pollutants). Such sources have been recognized by public authorities and well researched by scientists. (Addo et al., 2012; Akopyan et al., 2018; Cabral Pinto et al.,

* Corresponding author. Key Laboratory of Geochemical Cycling of Carbon and Mercury in the Earth's Critical Zone, Institute of Geophysical & Geochemical Exploration, Chinese Academy of Geological Sciences, Langfang, 065000, China.
E-mail address: chenghangxin@igge.cn (H. Cheng).

https://doi.org/10.1016/j.apgeochem.2020.104712
Received 10 December 2019; Received in revised form 29 April 2020; Accepted 24 July 2020
Available online 9 August 2020

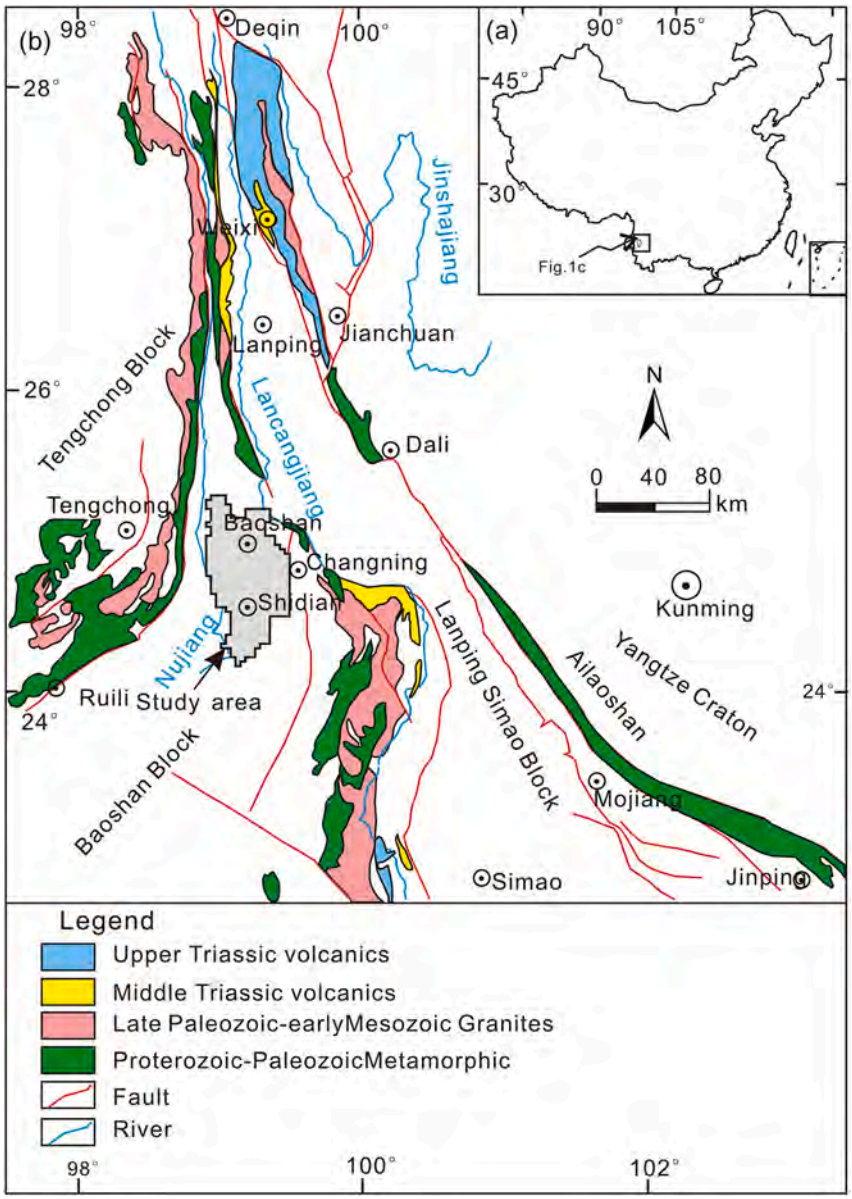

Fig. 1. Simplified tectonic map of Yunnan Sanjiang area (After Wang et al., 2010; Li et al., 2015).

2018, 2019a; 2019b; Chiu et al., 2016; Ettler, 2016; Hamzeh et al., 2011; Li et al., 2014a; Luo et al., 2012; McGrath and Tunney, 2010; Pinto et al., 2004; Poňavič et al., 2018; Rate, 2018). Soil can be naturally contaminated due to release of PTE from parent materials during weathering and this is evidenced by a significant body of research in this field e.g. (Antibachi et al., 2012; Becquer et al., 2006; Bompoti et al., 2015; Bonifacio et al., 2010; Kelepertzis et al., 2013; Tashakor et al., 2014). Therefore, it is crucial to understand geochemical fluxes in rock-soil systems, especially where the geological background (parent materials) are enriched in PTE. Understanding these fluxes will provide an important tool for assessing the natural environmental/ecological risk to soils. In this study, we examine geochemical fluxes at a regional scale. This has been achieved through the collection of rock samples from the host rock sequences, ore samples from Hetaoping copper-lead-zinc (HTP: Cu–Pb–Zn) and Heiyanao iron-copper-lead-zinc (HYA: Fe–Cu–Pb–Zn) mineral deposits, and their overlying soil samples. In this and other areas, the presence of carbonate and basalt parent materials often leads to elevated PTE in soil (Barsby et al., 2012; Cabral Pinto et al., 2017; Cheng, 2016; Cox et al., 2017; Goldhaber et al., 2009; Tolosana-Delgado and McKinley, 2016; Wang et al., 2015; Zhang et al., 2002).

In this study, compositional data analysis of the geochemical data for different geological formations and their overlying soils was used to (1) reveal the concentration of PTE in the rock-soil systems, (2) evaluate the enrichment and depletion of PTE in soils related to their underlying rock formations, (3) understand the transfer processes of PTE from rocks to soils, and (4) evaluate ecological risk and provide ecological risk prediction to similar geological areas. A comparison is provided with the index of geo-accumulation (I_{geo}) and enrichment factors (EF) which are have been used previously to assess baseline levels of contamination in the study area.

2. Research area

The Baoshan area is located in southwest China in the Yunnan province (Fig. 1a). The area has a mild subtropical climate that is tempered by its low latitude and moderate elevation. Baoshan has short, mild, dry winters, and warm, rainy summers. Contour maps of altitude, average surface soil temperature and rainfall are shown in Fig. 2. Variations in average temperature are directly related to altitude, whilst

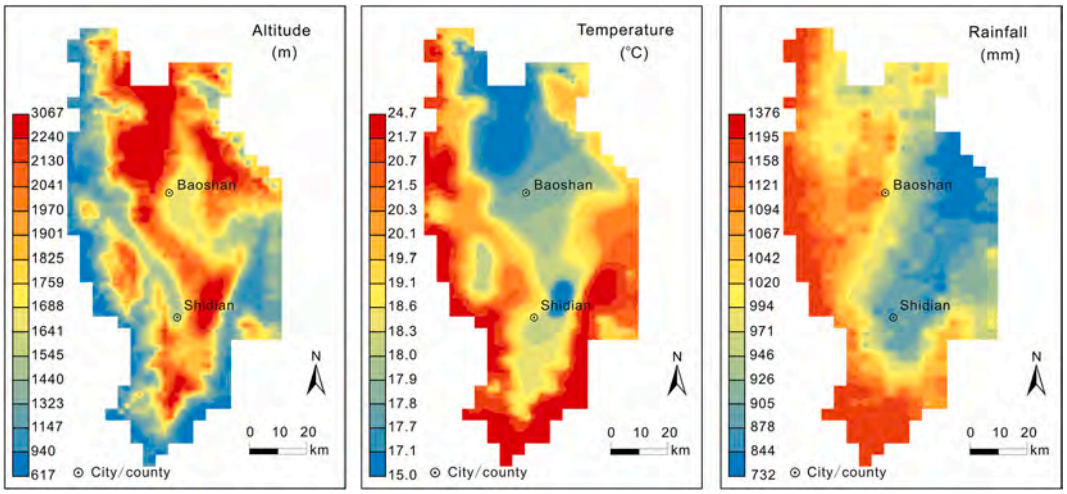

Fig. 2. Contour maps of altitude, average surface soil (0 cm) temperature and annual rainfall for study area.
(Altitude data, surface soil temperature data and rainfall data from National Earth System Science Data Sharing Infrastructure, National Science & Technology Infrastructure of China (http://www.geodata.cn)).

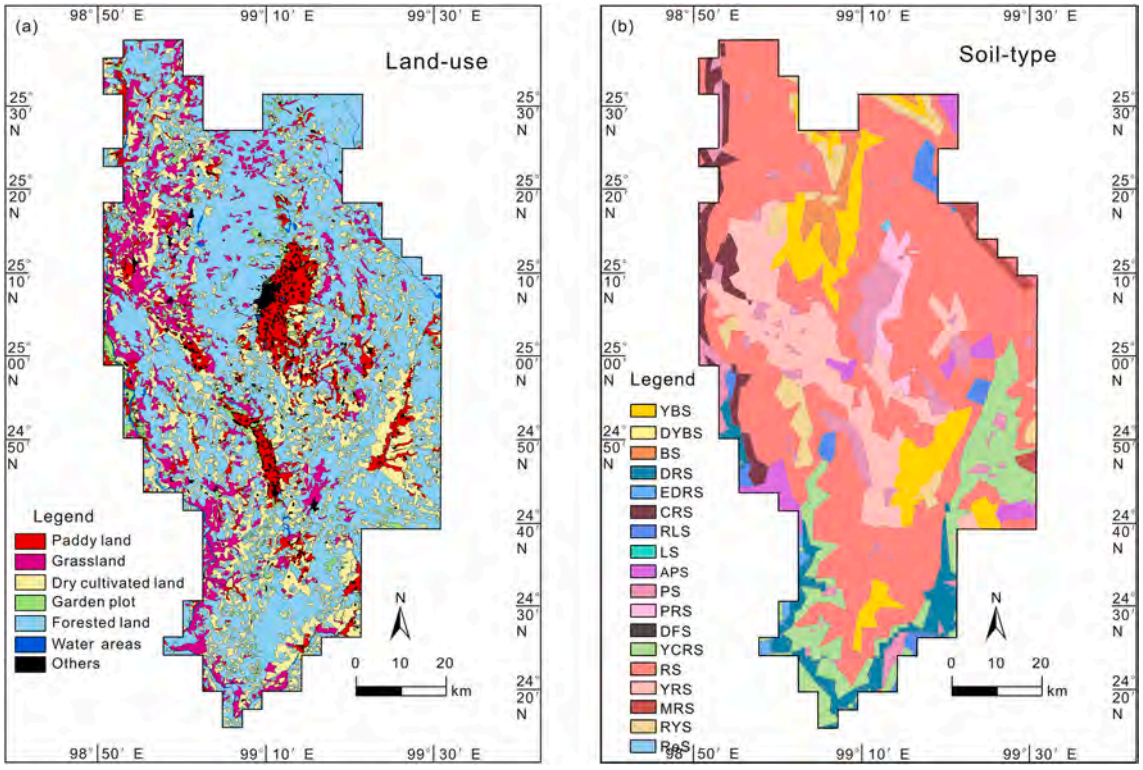

Fig. 3. Simplified land-use (a) and soil-type (b) maps of study area.
YBS: yellow brown soils; DYBS: dark yellow brown soils; BS: brown soils; DRS: dry red soils; EDRS: eluvial dry laterite; CRS: cinnamon red soils; RLS: red lime soils; LS: lime soils; APS: acid purple soils; PS: paddy soils; PRS: permeate rice soils; DFS: dark felty soils; YCRS: yellow crimson red soils; RS: red soils; YRS: yellow red soils; MRS: mountain red soils; RYS: rinse yellow soils; ReS: reservoir soils. (For interpretation of the references to colour in this figure legend, the reader is referred to the Web version of this article.)

rainfall is greatest in the western and southern parts of the study area. The main types of land-use in the study area are forested land, dry cultivated land, paddy land, grassland, garden plot, with few water areas and other types (residential quarter and industrial and mining land, and un-used land) (Fig. 3a). The main soil types in the study area are red soils, yellow red soils, yellow crimson red soils, dry red soils, yellow brown soils, dark yellow brown soils, paddy soils with few brown soils, acid purple soils and other types (Fig. 3b).

Geologically, the area is located in the Sanjiang area of the Yunnan province, which consists of the Tengchong, Baoshan, and Lanping-Simao blocks (Fig. 1b) (Dong et al., 2013; Li et al., 2015; Wang et al., 2010). Rocks of the Baoshan Block are mainly Paleozoic to Mesozoic sedimentary rocks, and early Paleozoic and late Mesozoic-early Cenozoic igneous rocks (Dong et al., 2013; Wang et al., 2013). From the Precambrian to Quaternary, the main rock type for each era is shown in Fig. 4. Basalt occurs in the Carboniferous and Jurassic rock sequences mainly distributed in the western and northeast parts of the study area. Whilst mineral deposits, which are often associated with PTE pollution

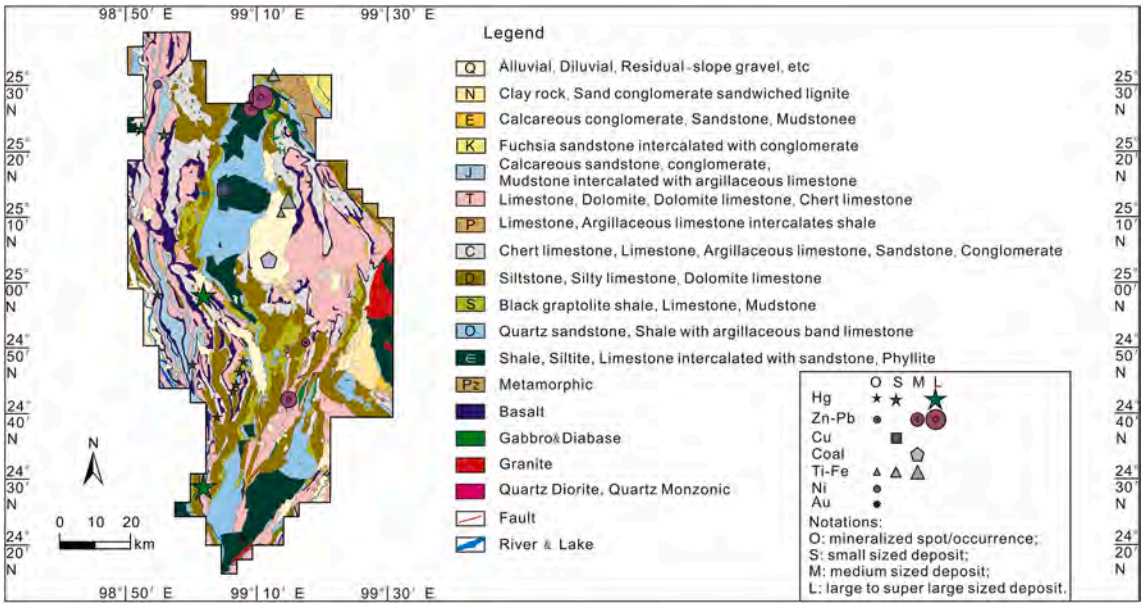

Fig. 4. Simplified geological and mineral deposits map of study area (After Zhang et al., 2020).

Table 1
Brief description of sampled rocks and their underlying geological formations in the Baoshan area.

No.	Sample Name	Formation Name	Sampled geological formation and deposit description	Age/ formation	Outcrop locations	Sampled rock (number)
1	Є-1-R	Є-1	Baoshan formation: Gray, yellow-green shale, sandstone containing limestone, argillaceous limestone; The lower section of Liushui formation: Yellow-green, grayish yellow siltstone, mudstone with argillaceous limestone	$Є_3b$; $Є_3l^1$	The northernmost part of the middle line in the study area	Mudstone (9); limestone (1)
2	Є-2-R	Є-2	Upper section of Shahechang formation: shale and siltstone; Hetaoping formation: grayish green slate; The upper section of the Shuangmai formation: dark green rhythmic slate	$Є_3s^2$; $Є_3h$; $Є_{1\text{-}2}sh^3$	North Central of the study area and northwest of Baoshan city	Mudstone (9); phyllite (2)
3	Є-3-R	Є-3	The upper section of Baoshan formation: shale, limestone with sandstone	$Є_3b^2$	Central part of the study area	Limestone (8); siliceous limestone (2)
4	O-R	O	Mantang formation: grayish white sandstone, shale (slate)	O_1m	Central north and south part of the study area	Sandstone (2); mudstone (4); quartz sandstone (4)
5	S-R	S	Upper Renheqiao formation: light gray reticulated limestone; Lower Renheqiao formation: Black graptolite shale	S_1r; S_2r	Distributed in the middle as narrow strip of the study area	Shale (7); limestone (3)
6	D-R	D	Shabajiao formation, Wangjiacun formation and Xiangyangsi formation are combined or not divided: sandy dolomite, argillaceous limestone, sandy limestone; Heyuanzhai formation: argillaceous limestone, pimple limestone; Dazhaimen formation: argillaceous limestone and calcareous mudstone	D_1; D_2hy; D_3d	Widely distributed in the central south and northwest	Limestone (9); dolomite (1); siltstone (1)
7	C-R	C	Pumenqian formation and Xiangshan formation are combined or not divided: Olitic limestone, chert limestone, mud limestone with argillaceous limestone in its lower part; Dingjiazhai formation: gray mudstone with argillaceous limestone, sandstone and conglomerate	C_1; C_3d	Midwest and northwest	Limestone (8); siliceous limestone (1); mudstone (1)
8	T-1-R	T-1	The upper section of Dashuitang formation: limestone, chert limestone	T_3d^2	Widely distributed in the west and east part of the study area	Limestone (8); dolomitic limestone (1); dolomite (1)
9	T-2-R	T-2	Hewanjie formation: dolomite	T_2h	Widely distributed in the west and east part of the study area	Dolomite (10)
10	J-R	J	Liuwan formation: limestone, shale and shell limestone	J_2l	Distributed in the west of the study area as long strips	Limestone (7); siliceous limestone (1); sandstone (2)
11	Ba-1-R	Ba-1	Woniusi formation: dense and amygdaloid basalt with limestone lens	C_3w	Northwest and northeast of the study area	Basalt (10)
12	Ba-2-R	Ba-2	The upper section of Mengjia formation: Basalt	J_2m^2	Southwest of the study area	Basalt (10)
13	HTP-O	HTP	Hetaoping Cu–Pb–Zn deposit. Main ore minerals: Galena, Chalcopyrite, Sphalerite, Pyrite, Pyrrhotite.	HTP	The northernmost part of study area	(Galena) (Chalcopyrite) Sphalerite (10)
14	HYA-O	HYA	Heiyanao Fe–Cu–Pb–Zn deposit. Main ore minerals: Pyrite, Chalcopyrite, Pyrrhotite, Magnetite, Hematite, Galena, Sphalerite.	HYA	The northernmost part of study area	(Galena) (Chalcopyrite) Sphalerite (5); chalcopyrite (1); pyrite (1); magnetite (3)

Table 2
Brief description of soils sampled in the Baoshan area.

No.	Sample Name	Soil type and soil characteristic description	Average altitude	Land use types of sampled soils (number)	Under formation
1	Є-1-S	Yellow brown soils/dark yellow brown soils. Black brown, brown and earthy yellow fine grain loam.	2470 m	Forest land (10)	Є-1
2	Є-2-S	Brown/yellow brown soils. Brown, earthy yellow fine grain loam.	2672 m	Forest land (11)	Є-2
3	Є-3-S	Yellow-red soils/ Acid purple soils. Red, earthy yellow, fine-medium grain loam.	1989 m	Forest land (3); Forest land/ Shrubland (7)	Є-3
4	O–S	Red soils/dry red soils/yellow red soils. Brown, earthy yellow fine-medium grain loam.	1473 m	Dry Cultivated land (6); Forest land/ Shrubland (4)	O
5	S–S	Yellow red soils/ red soils. Earthy yellow, red and brown fine-medium grain loam.	1876 m	Dry Cultivated land (6); Forest land/ Shrubland (4)	S
6	D-S	Yellow red soils/ red soils/acid purple soils. Earthy yellow and brown fine-medium grain loam.	1981 m	Dry Cultivated land (7); Forest land/ Shrubland (4)	D
7	C–S	Red soils. Brown, yellow brown, brick-red and earthy yellow fine grain loam.	2205 m	Dry Cultivated land (4); Forest land/ Shrubland (6)	C
8	T-1-S	Red soils. Brown, brick-red and earthy yellow fine-coarse grain loam.	2018 m	Dry Cultivated land (7); Forest land/ Shrubland (3)	T-1
9	T-2-S	Red soils. Red and brown fine-medium grain loam.	1835 m	Dry Cultivated land (7); Forest land/ Shrubland (3)	T-2
10	J-S	Phaeozems/red soils. Earthy yellow fine-medium grain loam.	861 m	Dry Cultivated land (2); Forest land/ Shrubland (8)	J
11	Ba-1-S	Red soils. Brown fine grain loam.	1708 m	Dry Cultivated land (4); Forest land/ Shrubland (6)	Ba-1
12	Ba-2-S	Phaeozems/red soils. Brown fine grain loam. The thickness of soil is extremely thin.	958 m	Wasteland (4); Forest land/ Shrubland (6)	Ba-2
13	HTP-S	Red soils. Brown fine grain loam.	2151 m	Forest land (10)	HTP
14	HYA-S	Yellow brown soils. Brown fine grain loam.	1966 m	Forest land/ Shrubland (10)	HYA

in soil, are widely distributed across the study area (copper, lead, zinc, mercury, gold, titanium and coal, etc.) (Fig. 4).

3. Methodology

3.1. Sampling methods

An area of 6220 km^2 of the 2016 National Geochemistry Survey of Land Quality project (NGSLQ) was selected as the research area because of the range of bedrock geology and mineralization present (Zhang et al., 2020). Samples of bedrock from all the main rock groupings and their overlying soils were collected. Additionally, ore samples from two deposits (the Hetaoping copper-lead-zinc deposit (HTP) and Heiyanao iron-copper-lead-zinc deposit (HYA)) and their overlying soils were also taken.

The sampling locations did not follow a predetermined pattern, as their selection required finding bedrock outcrops with or without mineralization and overlying soil. In total 102 rock samples from 12 geological formations, including 20 rock samples from the two basalt formations (Carboniferous and Jurassic), and 20 mineralized samples were collected. The sample details are provided in Table 1. Corresponding surface soil for each rock/ore sample, at 0–20 cm depth, were collected. Soil samples were composited from 3 to 5 subsamples collected within 50 m of each of the bedrock sample sites. Soil samples were ≥1 Kg, and visible plant detritus and rock fragments were removed during collection. The detailed soil type, soil characteristic, parent rocks/formations, and sample numbers are showed in Table 2. All the sampling positions were pinpointed by the Global Positioning System (GPS). The sample locations are shown in Fig. 5.

Obvious mineral vein material was removed from the rock samples. Samples were then ground using an agate mortar to −200 mesh (<0.074 mm) for analysis. The soil samples were disaggregated using a wooden hammer during air-drying and sieved with −20 mesh screen (<0.84 mm), once dried they were further processed to −200 mesh (<0.074 mm) for total content elements analysis and −100 mesh (<0.25 mm) for extractable As, Cd and Pb analysis.

3.2. Chemical analysis and quality control

Rock/ore and soil samples were analyzed for total content by XRF (Al_2O_3, TFe_2O_3, K_2O, SiO_2, Na_2O, MgO and CaO) after digestion by lithium tetraborate ($Li_2B_4O_7$); by XRF (Zr and Hf) after powder pressing; by ICP-OES (Ba, Ni, Sr and Cr) and ICP-MS (Cd, Cu, Cs, Pb, Rb, Ta, Th, U, Zn and Nb), after digestion by hydrofluoric acid (HF), hydrochloric acid (HCl), nitric acid (HNO_3) and perchloric acid ($HClO_4$); by AFS (As and Hg) after digestion with aqua regia; by HFIR (S), add tungsten grain in high-frequency infrared carbon sulfur meter; by VOL (C.org) after digestion by potassium dichromate ($K_2Cr_2O_7$) and concentrated sulfuric acid (H_2SO_4); and by ISE (pH) after dissolved in CO_2 distilled water. Extractable As, Cd and Pb from soil samples were digested using calcium chloride ($CaCl_2$) if the pH value ≤ 6.50, or digested using diethylenetriaminepentaacetic acid (DTPA) if the pH value > 6.50, then analyzed by AFS (As) and ICP-MS (Cd and Pb). Analyses were completed at the Hubei Geological Research Laboratory, which is one of the geological laboratories by accredited by the NGSLQ project. The analytical methods, brand and the model of analysis devices, and detection limits were listed in Table 3. Internal and external controls were implemented during routine analysis to check analysis accuracy and precision. Briefly, certified reference materials (CRMs) and blind reference materials (BRMs) were analyzed with samples simultaneously to control the quality of sample analysis. The detailed description can be seen in (Li et al., 2014b). The accuracies and precisions of all elements in all samples satisfy the analytical requirements developed in the NGSLQ project (CGS, 2005, 2014) and Code of Geochemical Rock Survey of China (Ministry of Land and Resources of the People's Republic of China, 2014).

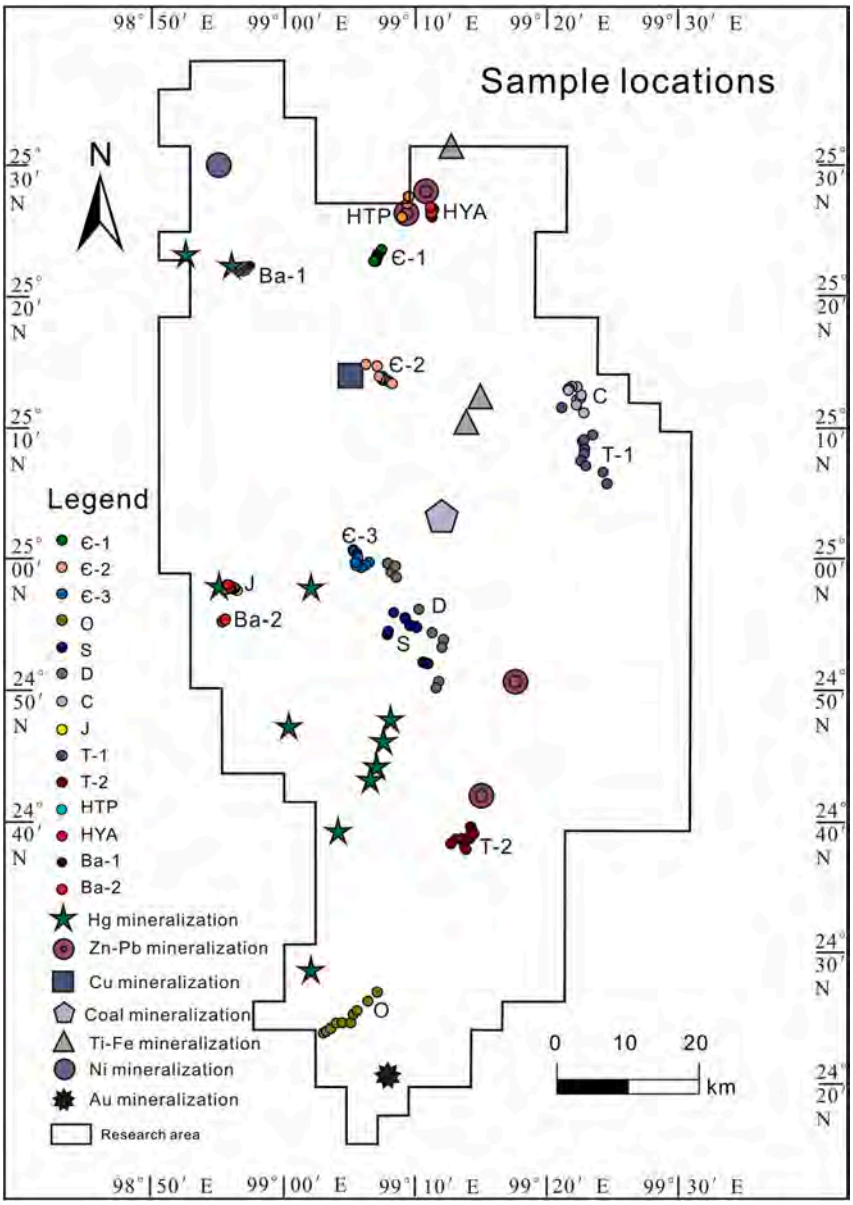

Fig. 5. Sample locations in each geological formation and near the HTP and HYA mining areas in this study. Deposit locations also showed in this map.

3.3. Statistical analysis

Geochemical data are compositional data, in that concentrations of each element cannot change independently and freely, but must accommodate each other within the constant sum constraint of the closed composition. Compositional data analysis methods have been developed which take account for the relative nature of compositional data (Aitchison, 1981, 1982, 1986; Boogaart and Tolosana-Delgado, 2013; Chayes, 1960; Egozcue et al., 2003; Pawlowsky-Glahn and Buccianti, 2011; Pawlowsky-Glahn and Egozcue, 2001).

In this paper, centred log-ratio transformation (clr) are used in CoDAPack to "open" the raw data, before any further statistical analysis. CoDAPack is a freeware package that implements most of the basic statistical methods suitable for compositional data (Thio-Henestrosa and Martin-Fernandez, 2006). Origin 2020 software was used for principal component analysis (PCA) on the log-ratio (clr) transformed data, Clr biplots are used to determine the associations of chemical elements.

4. Results and discussion

4.1. Chemical characteristics of rocks and soils

4.1.1. Rocks

Within the study area, the formations are distinguished based on the main rock type and these differ for most of the formations. Average (median value) concentrations of chemical elements of rocks from different geological formations and ores of the Baoshan area are shown in Table 4. Formations with carbonate rocks as their main rock type (Є-3, D, C, T-1, T-2 and J), those with mudstone and sandstone as main rock types (Є-1, Є-2, O and S), those with basalts (Ba-1 and Ba-2), and ores from mineral deposits (HTP and HYA), all display different chemical characteristics.

The carbonate formations have higher median values of CaO and Sr, and lower Al_2O_3, Fe_2O_3, MgO, SiO_2, Ba, Cr, Cs, Cu, Hf, Nb, Ni, Pb, Rb, Ta, Th, U, Zn and Zr compared to other formations apart from dolomite (T-2) which has the highest MgO content. Basalt formations have higher median values of Fe_2O_3, CaO, Na_2O, MgO, Cr, Cu, Ni and Sr, and lower Cs, Rb, Th, U contents compared to other formations. Mudstone and

Table 3
Analytical methods, devices, and detection limits.

Indicator	Analytical method	Brand and the model of analysis device	Detection limit	Unit	Sample
Al_2O_3	XRF	Shimadzu; XRF-1800X	0.03	wt. %	Rock and soil
CaO	XRF	Shimadzu; XRF-1800X	0.02	wt. %	Rock and soil
TFe_2O_3	XRF	Shimadzu; XRF-1800X	0.02	wt. %	Rock and soil
K_2O	XRF	Shimadzu; XRF-1800X	0.03	wt. %	Rock and soil
Na_2O	XRF	Shimadzu; XRF-1800X	0.02	wt. %	Rock and soil
MgO	XRF	Shimadzu; XRF-1800X	0.02	wt. %	Rock and soil
SiO_2	XRF	Shimadzu; XRF-1800X	0.05	wt. %	Rock and soil
As	AFS	Jitian; AFS-820	0.2	μg/g	Rock and soil
Ba	ICP-OES	ThermoFisher; ICAP6300	5	μg/g	Rock and soil
Cd	ICP-MS	ThermoFisher; X2	0.02	μg/g	Rock and soil
Cr	ICP-OES	ThermoFisher; ICAP6300	1.5	μg/g	Rock and soil
Cs	ICP-MS	ThermoFisher; X2	0.2	μg/g	Rock and soil
Cu	ICP-MS	ThermoFisher; X2	0.1	μg/g	Rock and soil
Hf	XRF	Shimadzu; XRF-1800X	0.1	μg/g	Rock and soil
Hg	AFS	Jitian; AFS-820	0.0005	μg/g	Rock and soil
Nb	ICP-MS	ThermoFisher; X2	1.4	μg/g	Rock and soil
Ni	ICP-OES	ThermoFisher; ICAP6300	0.2	μg/g	Rock and soil
Pb	ICP-MS	ThermoFisher; X2	0.2	μg/g	Rock and soil
Rb	ICP-MS	ThermoFisher; X2	0.1	μg/g	Rock and soil
S	HFIR	Saiensi; HCS-801A	15	μg/g	Rock and soil
Sr	ICP-OES	ThermoFisher; ICAP6300	2	μg/g	Rock and soil
Ta	ICP-MS	ThermoFisher; X2	0.1	μg/g	Rock and soil
Th	ICP-MS	ThermoFisher; X2	0.2	μg/g	Rock and soil
U	ICP-MS	ThermoFisher; X2	0.02	μg/g	Rock and soil
Zn	ICP-MS	ThermoFisher; X2	1	μg/g	Rock and soil
Zr	XRF	Shimadzu; XRF-1800X	1.5	μg/g	Rock and soil
C.org	VOL	–	0.02	μg/g	Soil
pH	ISE	Leici; PHS-3C	0.01	–	Soil
Extractable As	AFS	Jitian; AFS-820	0.01	μg/g	Soil
Extractable Cd	ICP-MS	ThermoFisher; X2	0.001	μg/g	Soil
Extractable Pb	ICP-MS	ThermoFisher; X2	0.004	μg/g	Soil

XRF: X-Ray Fluorescence Spectrometry; AFS: Cold Vapor-Atomic Fluorescence Spectrometry; ICP-MS: Inductively Coupled Plasma-Mass Spectrometry; ICP-OES: Inductively Coupled Plasma-Optical Emission Spectroscopy; HFIR: High frequency combustion infrared absorption; VOL: volumetric; ISE: Ion Selective Electrode; wt. %: Weight percent.

sandstone formations have higher median value of K_2O, SiO_2, Ba, Cs, Nb, Rb, Ta, Th, U and Zr, and lower CaO and Sr. Ore samples from the HTP and HYA mining areas have the highest median values of Fe_2O_3, As, Hg, Cd, Cu, Pb, Zn, and S.

To identify geochemical associations between the elements analyzed in the rocks and ores, PCA was performed using the centred log-ratio transformed (clr) data. The numerical output with the eigenvalues ≥1 (PC1: 46.9% of variance, PC2: 19.1% of variance, PC3: 11.7% of variance, and PC4: 4.5% of variance) of principal components captured potentially useful information and are listed in (Table 5), but only the first 3 principal components are examined here. The biplots of the principal components for the clr-transformed data of rocks and ores are shown in Fig. 6. With the aid of Table 5 and Fig. 6, the following observations have been made.

PC1 has positive contributions from As, Cd, Hg, Pb, Zn and S, and negative from Al_2O_3, Cr, Hf, Nb, Rb, Ta, Th, and Zr. PC2 has positive contributions from CaO, MgO and Sr, and negative from TFe_2O_3, Cu and SiO_2. PC3 has positive contributions from Cs, Rb, Th and U, and negative from Na_2O.

Several general elemental associations can be seen from component loadings in PC1-PC2, and PC1-PC3 space: chalcophile elements Cu, As, Cd, Hg, Pb, Zn and S occupied the +PC1/±PC2 quadrant (Fig. 6a) and are related to ore samples from HTP and HYA which clearly shows the influence of mineralization and its typical ore minerals such as galena (Pb, S), chalcopyrite (Cu, Fe, S), sphalerite (Zn, S), pyrite (Fe, S), chalcopyrite (Cu, Fe, S) pyrrhotite (Fe, S), magnetite (Fe), hematite (Fe, O). Arsenic and Hg are accessory elements that accompany Cu–Pb–Zn mineralization, whilst Cd normally replaces Zn due to their analogous nature (Alvarezayuso and Garciasanchez, 2003). The lithophile elements Al_2O_3, K_2O, SiO_2, Ba, Hf, Nb, Nb, Ta, Th, Zr, Cs and Rb occupied the -PC1/±PC2 quadrant (Fig. 6a) and clearly show the influence of mudstones and sandstones. Calcium (CaO), Sr, and MgO are grouped in the +PC1/+PC2 quadrant (Fig. 6a) and are related to the carbonate formations (Є-3, D, C, T-1, T-2 and J). The siderophile elements Fe, Cr, Ni and MgO occupied the -PC1/–PC3 quadrant (Fig. 6b) and are related to basalts.

4.1.2. Soils

The average (median value) concentrations of chemical components in soils overlying the rocks of different geological formations and near the HTP and HYA mining areas are showed in Table 6.

In general soils from the HTP and HYA mining areas have the highest As, Cd, Cu, Hg, Zn and Pb concentrations compared to those overlying other formations. However, the soils overlying carbonate rocks, also show As, Cd, Cu, Hg, Zn and Pb enrichment. Additionally, soils overlying carbonate rocks in the T-2 and J formations and those overlying the basalt formations (Ba-1 and Ba-2), have higher CaO, Sr and pH values compared to other formations. Conversely, soils overlying mudstone and sandstone formations (Є-1, Є-2, O and S) have lower CaO, Sr and pH values compared to other formations. The soils overlying basalt formations (Ba-1 and Ba-2) have higher TFe_2O_3, Na_2O, MgO, SiO_2, Cr and Ni, whilst those overlying carbonate formations show enrichment of Cr and Ni. The soils overlying mudstone and sandstone formations (Є-1 and Є-2) and those from the HTP and HYA mining areas have higher organic carbon (C.org) than other soils, whilst no obvious difference of C.org was found among soils overlying other formations.

The numerical output with the eigenvalues ≥1 (PC1: 33.3% of variance, PC2: 27.2% of variance, PC3: 9.0% of variance, and PC4: 8.0% of variance, PC5: 6.27% of variance, PC6: 3.87% of variance) from the principal component of soil are listed in Table 7. But only the first 3 principal components are examined here. With the aid of Table 7 and Fig. 7, the following observations were made.

PC1 has positive contributions from As, Cd, Cu, Pb and Zn, and negative from Al_2O_3, SiO_2, Hf, Nb, Ta, Th, U and Zr. PC2 has positive contributions from K_2O, Rb, Th and U, and negative from CaO, TFe_2O_3, Na_2O, MgO, Cr, Ni, Sr and pH. PC3 has negative contributions from Ba, S and C.org.

Several elemental associations were apparent from component loadings plotted in PC1-PC2, and PC2-PC3 space: chalcophile elements Cu, As, Cd, Hg, Pb, Zn and S occupy the +PC1/±PC2 quadrant (Fig. 7a)

Table 4
Average concentrations of major (wt.%) and trace elements (μg/g) for geological formations in the Baoshan area.

	UCC	Є-1-R	Є-2-R	Є-3-R	O-R	S-R	D-R	C-R	T-1-R	T-2-R	J-R	HTP-O	HYA-O	Ba-1-R	Ba-2-R
	Median	Median	Median	Median	Median	Median	Median	Median	Median	Median	Median	Median	Median	Median	Median
Al_2O_3	15.40	20.94	21.56	0.51	14.00	14.04	1.31	0.96	0.05	0.11	1.91	2.45	0.52	14.63	14.28
CaO	3.59	0.06	0.06	54.72	0.05	0.29	51.68	46.87	55.34	30.84	46.14	12.39	10.78	7.51	8.43
TFe_2O_3	5.04	7.87	9.25	0.34	3.70	4.62	0.57	0.45	0.04	0.21	1.54	17.79	30.01	12.42	13.36
K_2O	2.80	5.05	4.12	0.08	2.32	3.98	0.34	0.14	0.01	0.01	0.29	0.43	0.17	0.73	0.53
Na_2O	3.27	0.13	0.15	0.07	0.16	0.16	0.09	0.07	0.08	0.11	0.11	0.09	0.11	2.73	2.62
MgO	2.48	3.34	3.92	0.27	0.69	1.12	0.71	0.84	0.62	21.77	1.40	1.88	2.59	5.77	6.28
SiO_2	66.60	55.44	53.59	0.68	71.38	63.84	3.61	12.23	0.24	0.26	7.80	26.93	29.45	49.77	46.24
As	4.80	12.74	4.50	2.11	6.53	0.99	1.61	4.79	0.62	1.37	2.11	134.60	143.31	1.08	0.99
Ba	628.00	608.09	762.87	44.81	613.67	595.02	50.20	46.72	29.35	30.50	58.63	137.00	40.51	246.83	150.08
Cd	0.09	0.05	0.09	0.05	0.03	0.05	0.05	0.12	0.16	0.07	0.06	125.03	14.23	0.22	0.05
Cr	92.00	140.05	150.27	4.93	75.91	66.43	7.71	11.56	5.82	6.11	10.13	17.51	9.00	136.06	298.44
Cs	4.90	10.34	7.31	0.77	4.63	7.72	1.55	0.56	0.23	0.20	1.03	14.06	8.53	0.32	0.27
Cu	28.00	43.10	52.98	2.48	19.60	24.12	3.01	3.25	1.49	2.57	6.90	5500	571.24	124.68	61.65
Hf	5.30	2.45	2.60	0.55	6.60	5.65	0.90	1.00	0.65	0.40	0.70	4.35	0.85	3.15	2.95
Hg	0.05	0.02	0.01	0.12	0.02	0.01	0.01	0.05	0.03	0.07	0.02	0.76	0.18	0.03	0.01
Nb	12.00	16.15	15.81	0.59	13.18	12.43	2.48	1.70	0.44	0.28	1.59	1.46	0.63	9.97	8.89
Ni	47.00	61.54	69.33	1.95	21.13	33.43	3.97	4.17	1.99	1.48	7.78	8.61	2.86	67.99	271.45
Pb	17.00	10.54	12.20	7.18	10.00	9.39	3.39	3.09	2.41	4.27	10.96	54500	223.21	17.62	7.47
Rb	84.00	237.42	190.80	11.49	109.62	173.66	17.22	10.70	2.04	2.20	10.15	26.35	5.94	16.02	8.28
S	621.00	44.09	48.71	62.55	48.71	67.17	307.14	138.70	79.20	120.65	288.74	93500	13600	112.01	55.42
Sr	320.00	14.93	34.62	242.35	25.04	57.26	275.58	398.03	72.38	43.89	246.53	86.44	34.92	198.48	193.60
Ta	0.90	1.74	1.69	0.11	1.44	1.24	0.21	0.17	0.09	0.06	0.19	0.27	0.13	0.92	0.78
Th	10.50	22.27	21.94	2.73	18.18	18.32	2.99	3.75	0.53	0.96	1.60	2.49	0.91	2.98	2.32
U	2.70	2.34	2.75	0.57	2.73	2.49	0.60	0.66	0.86	0.83	0.84	0.68	0.49	0.51	0.44
Zn	67.00	99.32	118.62	11.93	40.58	41.78	18.68	15.15	6.18	13.93	27.63	63490	7856.30	136.49	107.73
Zr	193.00	99.05	98.10	7.95	216.50	198.60	20.70	17.20	5.50	4.20	17.00	103	4.90	110.70	103.65

UCC: upper continental crust (Rudnick and Gao, 2003).

Table 5
Variance explained by each principal component and component loadings for PC1-PC4 of rock/ore samples.

	PC1	PC2	PC3	PC4
Percentage of Variance	46.9%	19.1%	11.7%	4.5%
Cumulative Percent	46.9%	66.0%	77.7%	82.2%
Al_2O_3	−0.24	−0.18	−0.08	0.11
CaO	0.12	0.37	−0.07	0.17
TFe_2O_3	0.01	−0.35	−0.24	−0.12
K_2O	−0.21	−0.23	0.14	0.02
Na_2O	−0.12	0.19	−0.37	−0.09
MgO	−0.01	0.27	−0.17	−0.57
SiO_2	−0.13	−0.30	−0.12	0.25
As	0.21	−0.06	0.18	−0.09
Ba	−0.21	−0.05	0.18	−0.25
Cd	0.27	−0.04	0.01	0.01
Cr	−0.23	0.01	−0.22	−0.20
Cs	0.02	−0.18	0.45	−0.15
Cu	0.16	−0.28	−0.17	−0.10
Hf	−0.18	0.13	0.02	0.35
Hg	0.21	0.20	0.15	−0.00
Nb	−0.28	−0.02	−0.02	0.07
Ni	−0.22	−0.03	−0.28	−0.15
Pb	0.23	−0.13	0.03	0.12
Rb	−0.21	−0.08	0.35	−0.07
S	0.27	0.01	0.06	0.09
Sr	0.01	0.37	−0.05	0.30
Ta	−0.27	0.05	0.03	−0.03
Th	−0.23	0.05	0.26	−0.02
U	−0.12	0.25	0.29	−0.20
Zn	0.23	−0.23	−0.08	−0.06
Zr	−0.24	−0.02	−0.01	0.30

and are related to soil samples from near the HTP and HYA deposits. The lithophile elements Al_2O_3, SiO_2, K_2O, Ba, Hf, Nb, Rb, Ta, Th, U, Zr, Cs and Rb occupy the -PC1/±PC2 quadrant (Fig. 7a) and are clearly related to sandstone and mudstone formations which are enriched in those lithophile elements, and soils from carbonate formations (Є-3, D, C and T-1) due to the coprecipitation of insoluble elements during weathering and soil formation processes.

Siderophile elements Fe, Cr and Ni and CaO and MgO and pH occupied the ±PC1/–PC2 quadrant (Fig. 7a), which are related to basalts, which are enriched in Fe, Cr, Ni, Mg and Ca compare to other rock types. Removal of mobile elements (e.g., Ca, Na, Mg and Sr) and coprecipitation and/or adsorption by Fe-oxy-hydroxides of the insoluble element (e.g., Cr and Ni) occurs under the influence of high pH values. The soils overlying carbonate formations J and T-2 may be enriched in Cr and Ni for this reason. Potential toxic elements (PTE) coprecipitation and/or adsorption by Fe-oxy-hydroxides during weathering and soil formation process was also found by other authors (Buccianti et al., 2015; Cabral Pinto et al., 2017; Caillaud et al., 2009; Hamon et al., 2004; Rate, 2018). Organics related elements (e.g., C.org and S) are related to soils forming from Є-1 and Є-2 formation and those near the HTP and HYA mining areas. Fine-grain minerals in soils formed from mudstones are conducive to the accumulation of organic matters. Another explanation is that lower temperatures in these higher altitude areas limit organic turnover, which results in their increased accumulation even under conditions of smaller productivity of organic related elements input (Leifeld et al., 2005; Wiesmeier et al., 2013).

4.2. Enrichment and depletion of PTE in soils related to parent materials

Table 8 shows the enrichment and depletion of PTE in the soils overlying each geological formation and near the mining areas in relation to the bedrock, determined by Eqs. (1) and (2)

$$\text{Ratio} = \frac{(GM^x)_{soil}}{(GM^x)_{rock}} \quad (1)$$

where GM^x is geometric mean of element x, "soil" indicates the that element in soil, subscript "rock" indicates that element in the bedrocks.

$$GM^x = \sqrt[n]{\prod_{i=1}^{n} x_i} \quad (2)$$

where x_i is the contents of element i in different sample, n is the total sample number in each geological formations.

Fig. 8 is presented to highlight the differences. Ratio<1 indicates that soils overlying a specific formation are depleted in selected element and ratio>1 indicates that the soils are enriched. Soils overlying each geological formation, tend to be enriched in insoluble elements and depleted soluble elements related to the parent materials, and the amount of depletion is particularly significant in soils overlying carbonate formations (Є-3, D, C, T-1, T-2 and J). Soil compositions show slightly different enrichment and depletion depending on their parent rock type.

Soils overlying basalts (Ba-2 and Ba-1) are enriched in As, Cd, Cs, Hg, Rb, Th and U, and depleted in Ca, Na, Mg and Sr, whilst other elements do not show obvious enrichment or depletion. Soils overlying mudstone and sandstone formations (Є-1, Є-2, O and S) are depleted in Ca (S), K (Є-2) and Mg (Є-2), and enriched in As, Cd, Hg, Pb and S. Soils overlying carbonate formations (Є-3, D, C-1, T-1, T-2 and J) are depleted in Ca, Sr and Mg (in T-2), and enriched in nearly all other elements. The depletion of soluble elements, such as Ca and Sr, is due to them being washed away during weathering. The enrichment in Hf, Nb, Rb, Ta, Th and U is due to

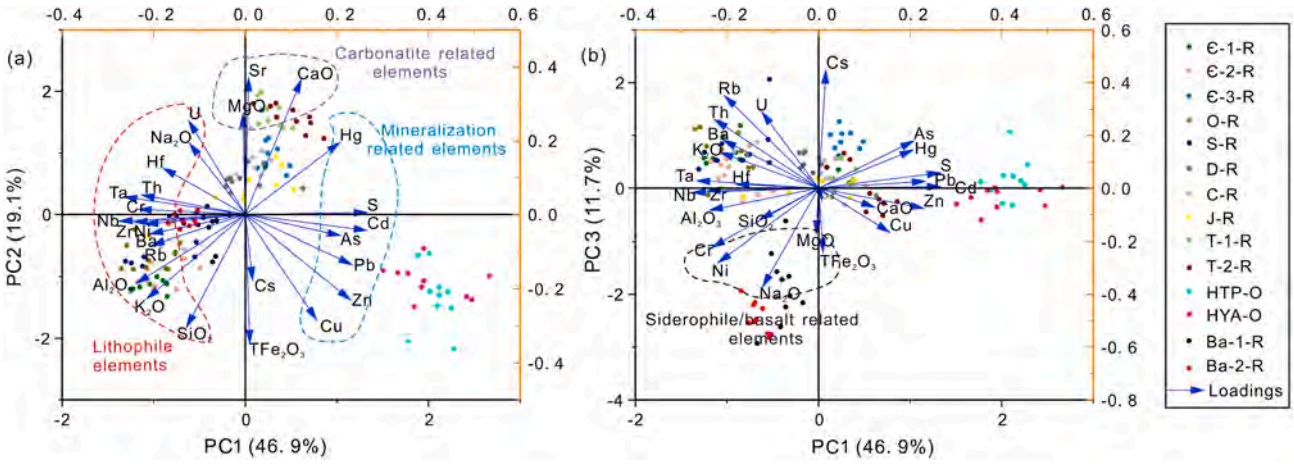

Fig. 6. Biplots of the principal components for the clr-transformed whole composition of rock and ore samples, with parallel plots for grouping of rock/ore samples by different geological formations in the PC1-PC2 (a) and PC1-PC3 (b) principal component space.

Table 6
Average concentrations of major (wt.%) and trace elements (μg/g) for soils developed on different geological formations in the Baoshan area.

	Deep soil of CGB	BL	Є-1-S	Є-2-S	Є-3-S	O–S	S–S	D-S	C–S	T-1-S	T-2-S	J-S	HTP-S	HYA-S	Ba-1-S	Ba-2-S
	Median	Median	Median	Median	Median	Median	Median	Median	Median	Median	Median	Median	Median	Median	Median	Median
Al_2O_3	11.9	18.29	19.88	18.87	23.36	17.25	18.70	18.01	16.06	25.38	20.20	15.31	18.11	18.57	14.38	16.15
CaO	2.57	0.62	0.24	0.16	0.29	0.09	0.26	0.50	0.37	0.62	3.63	10.02	2.04	0.59	4.35	6.30
TFe_2O_3	4.1	8.05	7.93	8.84	9.34	5.25	5.92	7.58	7.21	10.18	13.15	6.03	8.19	7.21	12.72	9.97
K_2O	2.36	2.56	2.77	2.06	2.70	2.78	3.58	3.38	0.91	1.36	1.27	2.31	1.91	3.13	0.65	1.44
Na_2O	1.81	0.17	0.15	0.16	0.13	0.16	0.11	0.11	0.10	0.12	0.10	0.26	0.25	0.15	1.36	0.29
MgO	1.36	1.28	1.27	1.24	0.78	0.54	1.19	1.20	0.65	1.07	3.16	1.96	2.48	2.17	4.47	2.33
SiO_2	67.9	59.68	50.16	49.06	49.90	66.27	61.32	57.79	61.47	44.74	39.79	47.80	45.92	53.28	44.78	46.40
As	9	18.73	17.16	10.02	30.72	7.57	8.26	14.08	28.42	28.58	26.00	12.05	196.19	166.62	1.27	6.17
Ba	522	341.60	382.65	435.26	305.27	538.13	467.65	319.19	167.63	257.18	163.96	248.37	599.92	855.50	158.38	258.31
Cd	0.11	0.13	0.21	0.21	0.22	0.10	0.11	0.15	0.37	3.61	0.57	0.16	4.51	7.44	0.11	0.14
Cr	50	119.00	111.93	115.50	133.40	94.26	98.89	119.46	116.75	164.16	190.05	92.63	113.42	112.31	196.85	184.53
Cs	6	–	14.00	9.36	21.24	6.19	11.14	16.46	7.10	16.99	12.12	8.54	15.24	13.03	1.19	5.50
Cu	19	45.19	43.86	41.12	64.07	28.46	28.84	30.08	47.96	63.17	71.86	30.42	162.39	623.57	124.71	49.51
Hf	6.1	–	3.90	3.70	6.60	8.25	7.25	8.50	5.20	6.95	4.30	3.85	4.10	7.40	2.70	3.70
Hg	0.018	0.11	0.20	0.23	0.58	0.05	0.06	0.06	0.20	0.27	0.51	0.03	0.34	0.40	0.02	0.02
Nb	12	20.19	17.28	19.72	24.06	18.26	20.73	35.45	26.69	26.89	26.89	14.19	15.79	21.20	11.79	15.16
Ni	22	57.74	44.95	32.94	72.19	28.03	43.35	50.64	75.53	110.16	59.59	48.43	65.99	64.76	64.53	132.72
Pb	21	30.65	48.93	37.93	123.16	28.80	28.95	38.54	30.73	66.48	98.96	19.13	334.16	2318.46	8.06	14.98
Rb	96	137.20	161.72	109.49	166.22	133.95	185.02	187.96	63.84	94.33	59.43	111.60	156.01	179.96	26.00	58.81
S	166	127.01	469.25	462.79	199.83	142.21	152.50	226.58	190.23	304.23	181.90	127.43	764.20	332.54	98.64	177.28
Sr	197	63.00	31.14	31.33	34.55	23.33	50.31	63.30	214.25	42.43	76.18	103.28	53.73	37.17	149.74	70.68
Ta	1	–	1.19	1.41	1.65	1.25	1.51	2.44	1.95	2.23	1.99	1.04	1.17	1.57	0.75	1.21
Th	10	15.69	20.25	19.84	26.35	18.36	20.99	22.14	17.61	21.73	12.24	11.30	17.12	20.20	3.93	7.54
U	2.4	3.08	3.09	3.06	3.60	3.36	3.06	3.58	3.60	4.72	4.13	2.20	1.96	2.60	0.62	1.73
Zn	60	100.25	119.19	84.35	195.10	43.01	77.17	100.25	139.94	219.28	183.51	68.75	574.92	3236.94	101.43	87.86
Zr	215	232.15	134.94	148.20	246.71	252.80	246.86	260.37	179.24	277.65	204.73	150.18	148.30	193.35	117.66	139.49
C.org	0.3	0.59	6.73	7.07	1.80	1.70	1.39	1.97	1.53	1.96	1.38	1.16	4.73	1.80	1.03	1.74
pH	8.1	6.57	5.13	5.06	5.61	5.18	5.61	6.39	5.75	6.66	7.99	8.36	7.33	6.80	6.91	8.19

Deep soil of CGB: the deep soil from China geochemical baseline project (CGB; Wang et al., 2016).
BL: background level, median value of deep soil from the 1:250000 scale land quality geochemistry survey of the study area (Zhang et al., 2020).

Table 7
Variance explained by each principal component and component loadings for PC1-PC6 of soil samples.

	PC1	PC2	PC3	PC4	PC5	PC6
Percentage of Variance	33.3%	27.2%	9.0%	8.0%	6.3%	3.9%
Cumulative Percent	33.3%	60.5%	69.5%	77.6%	83.9%	87.8%
Al_2O_3	−0.28	−0.08	0.02	0.03	−0.13	0.21
CaO	0.07	−0.27	−0.03	0.21	0.38	−0.04
TFe_2O_3	−0.14	−0.25	0.06	0.05	−0.30	0.21
K_2O	−0.18	0.19	−0.22	−0.11	0.29	0.29
Na_2O	−0.09	−0.28	−0.26	−0.12	−0.03	−0.02
MgO	0.01	−0.29	−0.17	0.06	0.12	0.07
SiO_2	−0.28	−0.04	−0.11	−0.15	−0.04	−0.16
As	0.21	0.21	0.14	0.06	0.00	−0.05
Ba	−0.09	0.13	−0.41	−0.34	0.00	0.06
Cd	0.28	0.05	0.11	−0.03	−0.03	−0.12
Cr	−0.17	−0.25	0.09	−0.01	−0.20	0.29
Cs	−0.04	0.27	0.14	0.19	0.20	0.35
Cu	0.20	−0.13	−0.03	−0.35	−0.22	0.06
Hf	−0.25	0.09	0.05	−0.25	0.05	−0.34
Hg	0.14	0.17	0.27	0.16	−0.26	0.07
Nb	−0.28	0.04	0.23	−0.02	−0.08	−0.14
Ni	−0.07	−0.26	0.23	−0.02	−0.08	0.34
Pb	0.24	0.19	0.03	−0.22	−0.05	0.00
Rb	−0.14	0.26	−0.16	−0.06	0.26	0.24
S	0.04	0.10	−0.35	0.41	−0.23	−0.13
Sr	−0.09	−0.25	0.07	0.10	0.17	−0.41
Ta	−0.26	0.05	0.26	0.06	−0.06	−0.09
Th	−0.20	0.27	0.04	0.01	−0.02	0.06
U	−0.20	0.20	0.18	0.15	0.03	−0.11
Zn	0.28	0.02	0.06	−0.29	−0.09	−0.02
Zr	−0.28	0.03	0.12	−0.18	0.01	−0.19
C.org	−0.05	0.09	−0.37	0.39	−0.27	−0.10
pH	0.12	−0.20	0.12	0.11	0.44	0.02

their low mobility during surface processes. The enrichment of Fe is due to its precipitation as oxy-hydroxides, whilst the enrichment of PTE (As, Cd, Cr, Cu, Hg, Ni, Pb and Zn) in the soils may be resulted by their coprecipitation and/or adsorption by Fe oxy-hydroxides (Buccianti et al., 2015; Cabral Pinto et al., 2017; Caillaud et al., 2009; Hamon et al., 2004; Rate, 2018).

Soils near the HTP and HYA mining areas are depleted in Ca, Fe, Cd, Cu (in HTP), Hg (in HTP), Pb (in HTP), S and Zn. Again, the depletion of Ca is because it easily mobilized and tends to be washed away during weathering. The depletion of other minerals is apparent and due to their high concentrations in the ore samples. Soils overlying HTP and HYA are enriched in Al, Cr, Hf, Nb, Ni, Rb, Ta, Th, U and Zr due to their coprecipitation during weathering.

4.3. Risk evaluation

Soils with the values of PTE (As, Cd, Cr, Cu, Hg, Ni, Pb and Zn) that exceed the risk screening values for soil contamination of agricultural land of the People's Republic of China (PRC) are listed in Table 9. If the concentration of PTE in agriculture land is lower than or equal to the risk screening values, the ecological risk of soils and environmental quality to agricultural products grown on the land are low, whereas if the concentration of PTE in agriculture land is higher than the risk screening values, the ecological risks for the soils and agricultural products grown in them is also high. Where the latter is the case soil environmental monitoring and collaborative testing of agricultural products should be executed (Ministry of Ecology and Environment of The People's Republic of China, 2018).

Most of the soil samples with PTE concentrations that exceed the risk screening values overly carbonate and basalt formations, or are from near the HTP and HYA mining areas.

For As, the samples mainly overly Є-3, C, T-1, T-2, HTP and HYA, with a few samples from the Є-1 and Є-2 formations. For Cd, the samples mainly overly the C, T-1, T-2, HTP and HYA. For Cr, the samples are mainly from over the T-1, T-2, Ba-1and Ba-2. For Cu, the samples mainly overly the Є-3, T-1, HTP, HYA and Ba-1. For Ni, the samples mainly overly Є-3, C-1, T-1, T-2, Ba-1 and Ba-2. For Pb and Zn, the samples mainly overly Є-3, HTP and HYA. Only two soil samples in study area are exceed the risk screening value of Hg, one overlies C-1 the other Є-3. As discussed previously, high levels of PTE in soil overlying basalt formations (Cr, Cu and Ni), and near HTP and HYA (As, Cd, Cu, Pb and Zn) are due to their high concentration in the bedrock. For soils overlying carbonate formations high levels are due to the coprecipitation (As, Cd, Cr, Cu, Hg, Ni, Pb and Zn) and/or adsorption by Fe-oxy-hydroxides under the influence of high pH values (e.g. Cr and Ni). Soils that form on carbonates and basalts, and in mining areas, have higher PTE content and higher ecological risk which has also been found by other researchers (Barsby et al., 2012; Cabral Pinto et al., 2017; Cheng, 2016; Cox et al., 2017; Goldhaber et al., 2009; Tolosana-Delgado and McKinley, 2016; Wang et al., 2015; Zhang et al., 2002).

The index of geo-accumulation (I_{geo}) and enrichment factors (EF) which are used widely to assess levels and origins of contamination (Barbieri, 2016; Bern et al., 2019; Cevik et al., 2009; Feng et al., 2011; Ghrefat et al., 2011; Liénard et al., 2014; Thiombane et al., 2019; Zhang et al., 2014). Reimann and Caritat (2000, 2005) and Sucharovà et al. (2012) have proposed that these indices cannot be used as rigorous, objective or sensitive tools to detect or prove anthropogenic impact on the environment due to the flaws of EF and I_{geo}. Whilst acknowledging the limitations of these indices due to the compositional nature of

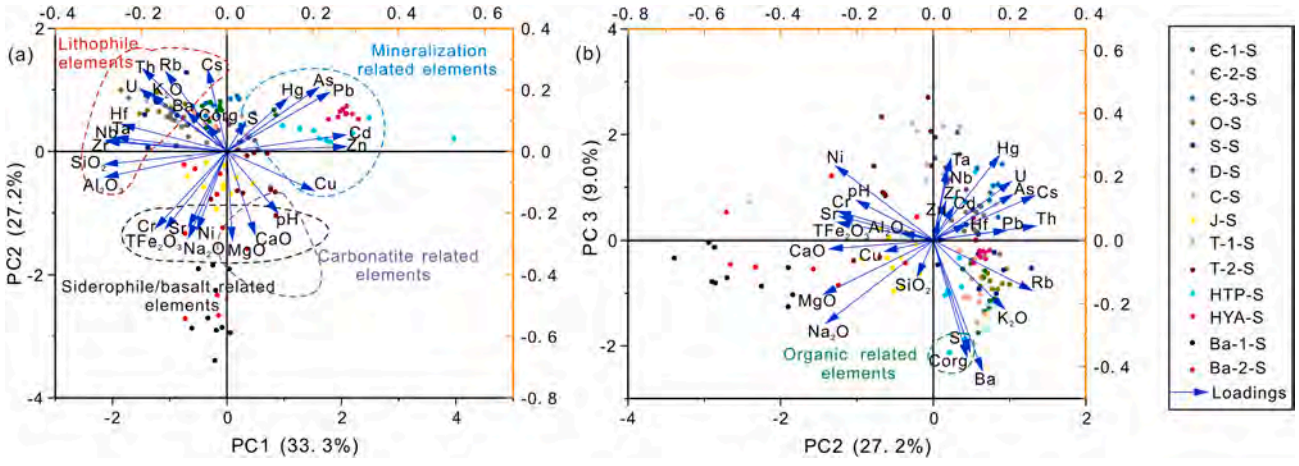

Fig. 7. Biplots of the principal components for the clr-transformed whole composition of soil samples, with parallel plots for grouping of soil samples by overlying different geological formations in the PC1-PC2 (a) and PC2-PC3 (b) principal component space.

Table 8
Level of enrichment/depletion of chemical elements from the Baoshan soils from the different geological formations, relatively to the respective rocks/ores.

	Є-1	Є-2	Є-3	O	S	D	C	T-1	T-2	J	HTP	HYA	Ba-1	Ba-2
Al_2O_3	1.35	0.92	52.25	1.28	1.57	13.68	11.76	372.70	243.37	6.64	7.28	34.87	1.01	1.13
CaO	2.78	2.70	0.01	1.65	0.19	0.01	0.03	0.02	0.10	0.47	0.31	0.05	0.56	0.65
TFe_2O_3	1.40	0.97	34.99	1.56	1.56	8.58	12.71	324.34	64.65	5.00	0.49	0.23	1.07	0.75
K_2O	0.86	0.58	33.84	1.09	1.13	9.76	8.24	112.25	86.36	6.22	4.55	18.99	0.74	2.93
Na_2O	1.11	0.57	1.89	0.64	0.72	1.24	1.47	1.64	0.86	1.54	2.57	1.35	0.61	0.14
MgO	0.62	0.34	2.53	0.95	1.07	1.03	1.21	0.69	0.15	1.13	1.56	1.00	0.77	0.42
SiO_2	1.28	0.91	120.64	0.92	1.35	13.32	4.07	229.84	174.94	4.23	1.61	1.88	0.90	0.92
As	3.77	3.93	16.17	1.72	5.37	7.01	6.23	39.00	19.26	5.04	1.99	1.00	1.03	6.24
Ba	0.85	0.60	6.39	0.99	0.96	6.25	2.78	10.40	4.49	3.12	2.64	18.54	0.84	1.43
Cd	5.59	1.91	4.42	2.86	2.20	2.23	2.78	20.77	8.46	2.39	0.03	0.37	0.54	2.32
Cr	1.11	0.81	26.47	1.40	1.66	11.86	6.87	25.02	23.89	5.85	6.29	12.89	1.46	0.65
Cs	1.70	1.13	28.68	1.47	1.61	10.19	7.54	61.15	50.63	8.55	1.28	1.41	1.95	17.95
Cu	1.42	0.83	24.67	1.41	1.52	8.42	11.21	37.40	20.44	3.64	0.05	0.78	1.13	0.75
Hf	1.77	1.39	12.95	1.27	1.46	8.92	3.75	13.30	11.09	3.00	1.61	11.02	0.93	1.19
Hg	16.91	17.51	5.93	2.22	3.20	3.95	4.44	14.83	4.93	2.50	0.61	1.54	0.96	2.54
Nb	1.47	1.21	40.61	1.53	1.80	14.07	10.05	63.40	77.05	6.98	10.24	34.77	1.25	1.66
Ni	1.09	0.52	34.31	1.08	1.69	10.01	10.33	58.77	40.42	5.20	6.64	22.90	1.04	0.58
Pb	6.21	3.26	13.16	2.81	3.34	9.50	7.24	27.63	17.23	1.82	0.01	8.56	0.40	1.94
Rb	1.03	0.63	15.63	1.17	1.30	8.99	4.07	47.93	24.62	8.20	6.34	32.16	1.50	8.54
S	10.26	8.09	2.74	2.32	1.72	0.49	0.95	3.46	1.68	0.73	0.01	0.02	0.81	2.49
Sr	1.32	0.80	0.13	0.79	0.72	0.28	0.50	0.60	1.77	0.50	0.78	1.01	0.72	0.37
Ta	0.92	0.86	14.32	1.02	1.42	9.12	7.00	25.04	23.69	4.32	4.23	11.43	0.85	1.36
Th	1.23	0.90	10.09	1.00	1.32	6.76	3.68	44.88	14.20	5.58	7.97	27.77	1.27	3.21
U	1.70	1.18	6.19	1.21	1.34	5.69	3.96	6.46	4.54	2.46	3.35	5.45	1.40	3.12
Zn	1.50	0.71	16.83	1.13	1.70	4.37	6.12	33.73	11.65	2.25	0.01	0.27	0.75	0.81
Zr	1.79	1.39	30.11	1.18	1.34	12.20	6.18	45.47	42.92	4.76	1.80	44.16	1.09	1.41

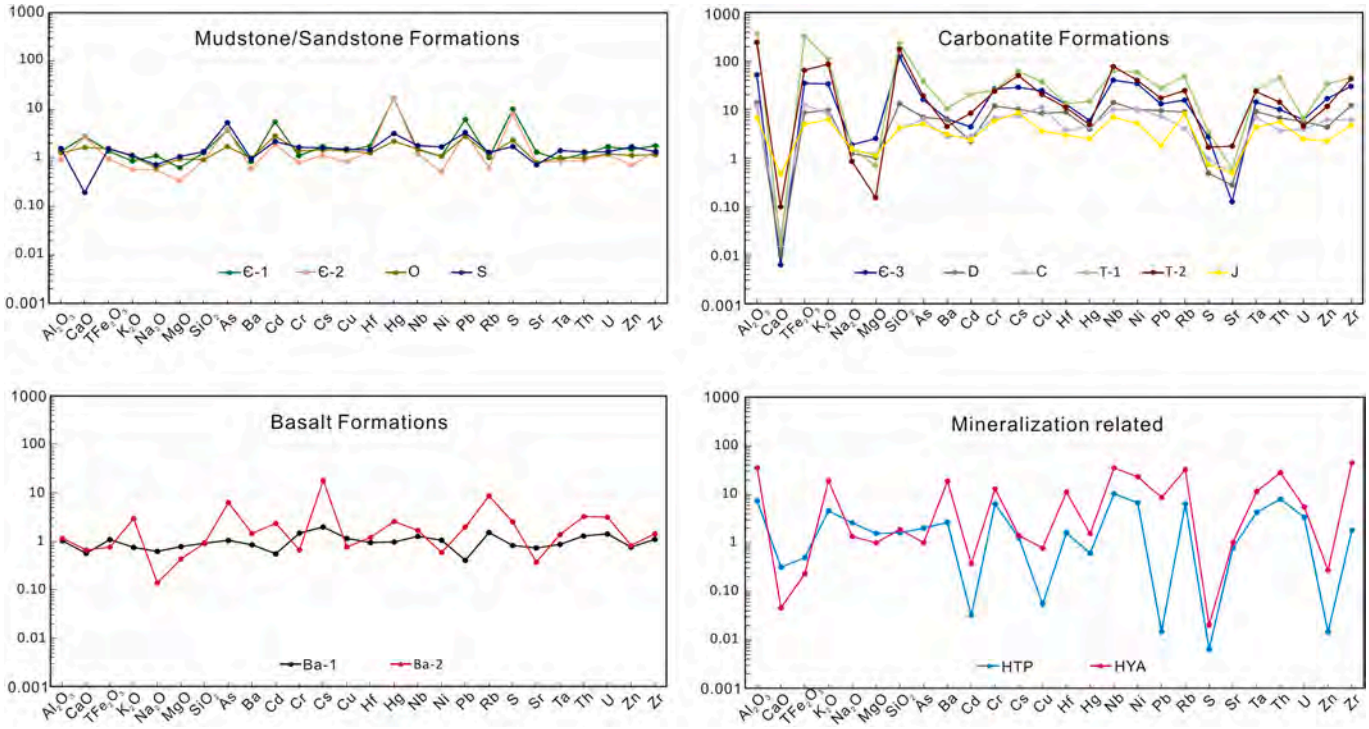

Fig. 8. Geometric mean of elements ratio (soil/rock) in derived from the different geological formations to reflect the PTE enrichment and depletion in soils related to their bedrocks.

geochemical data, these indexes are still widespread in their use to assess levels of contamination. This research attempts to use the results from compositional data analysis to highlight the limitations of the indices and provide an alternative approach assess levels of contamination and contribution of parental bedrock. As previous work in the area has been completed using these indices which has provided a baseline for soil environmental risk. Therefore, for completeness calculation of the current indices are provided below.

The I_{geo} and EF are calculated using the following equations (Eqs. (3) and (4)):

$$I_{geo} = \log 2\left[\frac{C_n}{1.5B_n}\right] \quad (3)$$

where C_n is the concentration for a given PTE and B_n is the background level of that PTE in the soil (Müller, 1969). The median values of PTE in deep soil from the 1:250000 scale land quality geochemistry survey in Baoshan area, as are much less likely to be affected by human activities

Table 9
Numbers of contaminated soil samples from different geological formations in the Baoshan area.

PTE	Methods		Numbers of contaminated soil samples													
			Є-1	Є-2	Є-3	O	S	D	C	T-1	T-2	J	HTP	HYA	Ba-1	Ba-2	Total
As	I_{geo}	Bn = BL	1	1	–	–	–	–	1	–	–	–	9	10	–	–	22
		Bn = CGB	2	1	1	–	–	–	4	–	2	–	10	10	–	–	30
	EF		6	7	–	3	7	1	–	–	–	2	1	–	3	10	40
	>RSV		4	3	6	–	–	–	6	6	5	–	10	10	–	–	50
Cd	I_{geo}	Bn = BL	2	–	–	–	–	–	2	10	3	–	9	10	–	–	36
		Bn = CGB	–	–	–	–	–	–	5	10	4	–	10	10	–	–	39
	EF		6	6	–	–	–	–	–	–	–	1	–	–	–	5	18
	>RSV		3	1	3	1	1	–	6	10	6	–	10	10	–	–	51
Cr	I_{geo}	Bn = BL	–	–	–	–	–	–	–	–	–	–	–	–	–	–	0
		Bn = CGB	–	–	–	–	–	–	1	–	–	–	–	–	3	2	6
	EF		–	–	–	–	–	1	–	–	–	–	–	–	–	3	4
	>RSV		–	1	1	–	1	1	1	4	3	–	–	–	5	4	17
Cu	I_{geo}	Bn = BL	–	–	–	–	–	–	–	–	–	–	–	–	–	–	0
		Bn = CGB	–	–	–	–	–	–	1	–	2	–	9	10	6	–	28
	EF		–	–	–	1	3	–	2	–	–	1	–	–	1	–	8
	>RSV		3	3	7	–	–	–	3	4	2	–	9	10	8	–	49
Hg	I_{geo}	Bn = BL	–	–	4	–	–	–	1	–	5	–	2	–	–	–	12
		Bn = CGB	10	10	11	–	2	1	7	10	8	1	10	10	–	–	79
	EF		10	10	–	4	6	–	1	–	–	3	–	–	2	5	41
	>RSV		–	–	1	–	–	–	1	–	–	–	–	–	–	–	2
Ni	I_{geo}	Bn = BL	–	–	–	–	–	–	–	–	–	–	–	–	–	–	0
		Bn = CGB	–	–	–	–	–	–	–	1	2	–	–	–	3	5	11
	EF		–	–	–	–	2	–	–	–	–	–	2	1	1	–	6
	>RSV		3	1	6	–	1	–	–	–	3	–	9	10	–	–	49
Pb	I_{geo}	Bn = BL	–	–	2	–	–	–	–	–	2	–	7	10	–	–	21
		Bn = CGB	–	1	4	–	–	–	–	–	3	–	9	10	–	–	27
	EF		10	10	–	5	4	–	2	–	–	–	–	1	–	4	36
	>RSV		1	2	9	–	1	–	–	–	3	–	9	10	–	–	35
Zn	I_{geo}	Bn = BL	–	–	–	–	–	–	–	–	–	–	4	10	–	–	14
		Bn = CGB	–	–	–	–	–	–	–	1	2	–	7	10	–	–	20
	EF		–	–	–	1	2	–	–	–	–	–	–	–	–	–	3
	>RSV		1	3	1	–	–	–	–	7	3	–	9	10	–	–	34

BL: background level, median value of deep soil from the 1:250000 scale land quality geochemistry survey of the study area (Zhang et al., 2020).
CGB: the median value of deep soil of China geochemical Baseline project (Wang et al., 2016).
RSV: the risk screening values for soil contamination of agricultural land of the People's Republic of China (Ministry of Ecology and Environment of The People's Republic of China, 2018).
Soils with the PTE I_{geo} index or EF value > 2 are thought to be contaminated in this study.

(Cheng et al., 2014c; Zhang et al., 2020) and geochemical background baseline of China, the median values of deep soil of China Geochemical Baseline project (Wang et al., 2016) were used as B_n for calculation separately.

$$EF = \frac{(Metal/RE)_{soil}}{(Metal/RE)_{rock}} \quad (4)$$

Where EF is the enrichment factor for a given PTE, subscript "soil" indicates surface soil concentration for that PTE, subscript "rock" indicates that PTE in the bedrocks, and "RE" is the concentration of reference element. Aluminum is choosing as RE for its non-mobile nature during weathering (Balls et al., 1997; Cabral Pinto et al., 2017; Ryan and Windom, 1988; Sinex and Wright, 1988).

The results of I_{geo} with the value > 2 are considered to be contaminated, according to previous studies (Müller, 1969; Odewande and Abimbola, 2008). The numerical results are shown in Table 9. The results of I_{geo} for As, Cd, Pb and Zn based on local background levels (median values of deep soil from the 1:250000 scale land quality

Table 10
Average concentrations of extractable As, Cd and Pb (μg/g), and their percentage to total content in the soils developed on different geological formations in the Baoshan.

	Extractable Cd	Ex Cd Ratio	Extractable Pb	Ex Pb Ratio	Extractable As	Ex As Ratio
	Median	Median	Median	Median	Median	Median
Є-1	0.022	0.116	0.039	0.001	–	–
Є-2	0.022	0.127	0.074	0.002	–	–
Є-3	0.022	0.097	0.104	0.001	–	–
O	0.019	0.198	0.049	0.002	–	–
S	0.014	0.161	0.113	0.004	–	–
D	0.016	0.127	0.137	0.005	–	–
C	0.024	0.087	0.144	0.022	–	–
T-1	0.250	0.068	3.012	0.043	–	–
T-2	0.103	0.158	6.773	0.071	–	–
J	0.015	0.086	0.879	0.051	–	–
HTP	0.794	0.119	17.511	0.052	–	–
HYA	1.657	0.222	631.620	0.289	0.001226248	0.00001
Ba-1	0.013	0.120	0.140	0.020	–	–
Ba-2	0.009	0.084	0.416	0.030	–	–

Ex Cd Ratio: Extractable ratio of Cd, calculated by $(Cd_{exteactable})/(Cd_{total\ content})$, same to Pb and As.

geochemistry survey in the Baoshan area) and geochemical background baseline of China (the median values of deep soil of China Geochemical Baseline project) do not show much difference. The soils with As, Pb and Zn contamination occur mainly near HTP and HYA mining areas; the soils with Cd contamination mainly from the C, T-1 and T-2 formations and soils near HTP and HYA mining areas. While, for elements Hg, Ni and Cu show different results base on the B_n. Use local background as B_n may underestimate the PTE contamination in where there is a high geological background of PTE. By conducting a comparison with larger-scale datasets as background when calculating this is a better way to solve the problem.

Normally, the value of $0.5 < EF < 1.5$ is taken as an indicator that PTE are entirely provided from natural contributions such as weathering, and a value of $EF > 1.5$ is considered to indicate the PTE are delivered from non-crustal materials, for example, biota and/or pollution drainage (Zhang and Liu, 2001). Combining the contamination categories (Addo et al., 2012; Barbieri, 2016; Loska et al., 2003), soils with EF value > 2 are thought to be moderately contaminated and caused by anthropogenic activities. The results in Table 9 show that, soils with As, Cd, Hg and Pb contamination are mainly overlying formations of Є-1, Є-2, O, S and Ba-2. Those contaminate sample locations according to EF value are mainly near mining areas (Fig. 3), and this may indicate that the mining activities led to soil contamination. While no contamination was found in the soils near HTP and HYA mining areas according to EF results. This is due to the high concentration of PTE (As, Cd, Hg, Pb and Zn) in ores. As such, the EF calculated for soil-rock in high geological background areas may underestimate the contamination.

Assessment of the concentration of bioavailable of PTE in soils is vital to evaluate soil quality (Barbieri, 2016; Barsby et al., 2012; Cox et al., 2017; Jackson et al., 2016; Palmer et al., 2014; Prathumratana et al., 2018; Zhang et al., 2018). For the reason, PTE in soil from anthropogenic origins tend to be more mobile, hence more bio-available than for pedogenic or lithogenic ones (Basta et al., 2005; Kuo et al., 1983; Nannoni et al., 2011). To find the biological risk of PTE, the extractable As, Cd and Pb of soil samples were analyzed, the results are showed in Table 10. Extractable As is not discussed further as results for most samples were lower than detection limits. The soils overly HTP and HYA have higher extractable Cd and Pb concentration and ratio than other soils (Table 10), which may indicate the contribution of mining activities to the surface soils contamination.

Based on the soil environmental assessment methods used above, we suggest that the monitoring of soils formed on carbonate rocks and basalts, and especially mineralization formations and mining areas should be implemented in this study area.

5. Conclusions

This research demonstrates enrichment of potential toxic elements (PTE) (As, Cd, Cr, Cu, Hg, Ni, Pb and Zn) in soils related to their parent materials. The enrichment in soils may be due to the removal of mobile elements (e.g., Ca, Na, Mg and Sr), and coprecipitation (As, Cd, Cr, Cu, Hg, Ni, Pb and Zn) and/or adsorption by Fe-oxy-hydroxides (Cr and Ni) under the influence of high pH values during soils formation. However, anthropogenic contamination is also possible for soil near mining areas. The soils forming from carbonate rocks, basalts, and especially mineralization formations have a higher PTE concentration, that exceeds risk screening values for soil contamination of agricultural land of China. Ecological monitoring should be implemented on those soils in the study area. This study reinforces issues found with the use of the commonly used approaches - the geo-accumulation index (I_{geo}) and enrichment factor (EF) methods. The approaches do not account for the compositional nature of the geochemical data and as a result were found to underestimate PTE contamination where there is a high geological background of PTE. A compositional data analysis approach (using clr biplots) shows that comparison with regional-scale background datasets is essential to provide a more informative approach to evaluate the risk of soil contamination, especially in regions with elevated levels of PTE in parent materials.

Declaration of competing interest

The authors declare that they have no known competing financial interests or personal relationships that could have appeared to influence the work reported in this paper.

Acknowledgements

The authors would like to thank the China Geological Survey (DD20160313), Ministry of Finance of China (121201108000168530) and China Scholarship Council (CSC201868110267) for funding. Thanks also to the Hubei Geological Research Laboratory, for their analysis the samples in this study. Acknowledgement for the data support from "National Earth System Science Data Sharing Infrastructure, National Science & Technology Infrastructure of China (http://www.geodata.cn)". Finally, the authors would like to express our sincere thanks to the editor and the anonymous reviewers for their critical and constructive comments and suggestions.

Appendix A. Supplementary data

Supplementary data to this article can be found online at https://doi.org/10.1016/j.apgeochem.2020.104712.

References

Addo, M., Darko, E., Gordon, C., Nyarko, B.J.B., Gbadago, J., Nyarko, E., Affum, H., Botwe, B., 2012. Evaluation of heavy metals contamination of soil and vegetation in the vicinity of a cement factory in the volta region, Ghana. Int. J. Sci. Technol. 2, 40–50.
Aitchison, J., 1981. A new approach to null correlations of proportions. J. Int. Assoc. Math. Geol. 13, 175–189.
Aitchison, J., 1982. The statistical analysis of compositional data. Technometrics 30, 120–121.
Aitchison, J., 1986. The Statistical Analysis of Compositional Data. Monographs on Statistics and Applied Probability. Chapman & Hall Ltd., London (UK), p. 416. London (UK) (Reprinted in 2003 with additional material by The Blackburn Press).
Akopyan, K., Petrosyan, V., Grigoryan, R., Melkomian, D.M., 2018. Assessment of residential soil contamination with arsenic and lead in mining and smelting towns of northern Armenia. J. Geochem. Explor. 184, 97–109.
Alvarezayuso, E., Garciasanchez, A., 2003. Sepiolite as a feasible soil additive for the immobilization of cadmium and zinc. Sci. Total Environ. 305, 1–12.
Antibachi, D., Kelepertzis, E., Kelepertsis, A., 2012. Heavy metals in agricultural soils of the mouriki-thiva area (Central Greece) and environmental impact implications. Soil Sediment Contam.: Int. J. 21, 434–450.
Balls, P.W., Hull, S., Miller, B.S., Pirie, J.M., Proctor, W., 1997. Trace metal in scottish estuarine and coastal sediments. Mar. Pollut. Bull. 34, 42–50.
Barbieri, M., 2016. The importance of enrichment factor (EF) and geoaccumulation index (Igeo) to evaluate the soil contamination. J. Geol. Geophys. 5.
Barsby, A., McKinley, J.M., Ofterdinger, U., Young, M., Cave, M.R., Wragg, J., 2012. Bioaccessibility of trace elements in soils in Northern Ireland. Sci. Total Environ. 433, 398–417.
Basta, N.T., Ryan, J.A., Chaney, R.L., 2005. Trace element chemistry in residual-treated soil: key concepts and metal bioavailability. J. Environ. Qual. 34, 49–63.
Becquer, T., Quantin, C., Rotte-Capet, S., Ghanbaja, J., Mustin, C., Herbillon, A.J., 2006. Sources of trace metals in Ferralsols in New Caledonia. Eur. J. Soil Sci. 57, 200–213.
Bern, C.R., Walton-Day, K., Naftz, D.L., 2019. Improved enrichment factor calculations through principal component analysis: examples from soils near breccia pipe uranium mines, Arizona, USA. Environ. Pollut. 248, 90–100.
Bompoti, N., Chrysochoou, M., Dermatas, D., 2015. Geochemical characterization of Greek ophiolitic environments using statistical analysis. Environmental Processes 2, 5–21.
Bonifacio, E., Falsone, G., Piazza, S., 2010. Linking Ni and Cr concentrations to soil mineralogy: does it help to assess metal contamination when the natural background is high? J. Soils Sediments 10, 1475–1486.
Boogaart, K.G.V.D., Tolosana-Delgado, R., 2013. Analyzing Compositional Data with R. Use R, pp. 73–93.
Buccianti, A., Lima, A., Albanese, S., Cannatelli, C., Esposito, R., De Vivo, B., 2015. Exploring topsoil geochemistry from the CoDA (compositional data analysis) perspective: the multi-element data archive of the campania region (southern Italy). J. Geochem. Explor. 159, 302–316.
Cabral Pinto, M.M.S., Silva, M.M.V.G., Ferreira da Silva, E.A., Dinis, P.A., Rocha, F., 2017. Transfer processes of potentially toxic elements (PTE) from rocks to soils and

the origin of PTE in soils: a case study on the island of Santiago (Cape Verde). J. Geochem. Explor. 183, 140–151.
Cabral-Pinto, M.M.S., Marinho-Reis, A.P., Almeida, A., Ordens, C.M., Silva, M.M., Freitas, S., Simoes, M.R., Moreira, P.I., Dinis, P.A., a Diniz, M.L., da Silva, E.A.F., de Melo, M.S.C., 2018. Human predisposition to cognitive impairment and its relation with environmental exposure to potentially toxic elements. Environ. Geochem. Health 40 (5), 1767–1784.
Cabral-Pinto, M.M., Inácio, M., Neves, O., Almeida, A.A., Pinto, E., Oliveiros, B., da Silva, E.A.F., 2019a. Human health risk assessment due to agricultural activities and crop consumption in the surroundings of an industrial area. Exposure and Health 1–12.
Cabral-Pinto, M.M.S., Ordens, C.M., de Melo, M.T.C., Inácio, M., Almeida, A., Pinto, E., da Silva, E.A.F., 2019b. An inter-disciplinary approach to evaluate human health risks due to long-term exposure to contaminated groundwater near a chemical complex. Exposure and Health 1–16.
Caillaud, J., Proust, D., Philippe, S., Fontaine, C., Fialin, M., 2009. Trace metals distribution from a serpentinite weathering at the scales of the weathering profile and its related weathering microsystems and clay minerals. Geoderma 149, 199–208.
Cevik, F., Goksu, M.Z., Derici, O.B., Findik, O., 2009. An assessment of metal pollution in surface sediments of Seyhan dam by using enrichment factor, geoaccumulation index and statistical analyses. Environ. Monit. Assess. 152, 309–317.
CGS, 2005. Technical requirements for sample analysis for eco-geochemical evaluation (DD2005-03). In: China Geological Survey. Beijing. (In Chinese).
CGS, 2014. Specification for multi-purpose regional geochemical survey (DD/T 0258-2014). In: China Geological Survey. Beijing. (In Chinese).
Chayes, F., 1960. On Correlation between Variables of Constant Sum. Revista De Economía Del Caribe, pp. 42–78, 1996.
Cheng, X.M., 2016. Geochemical Behavior and Risk Analysis for Heavy Elements in Soil Profiles with Different Parent Material, Yunnan Province, China. China University Of Geosciences, Beijing (In Chinese with English abstract).
Cheng, H., Li, M., Xie, X., Yang, Z., Li, C., 2014a. Exploring China: environment and resources. J. Geochem. Explor. 139, 1–3.
Cheng, H., Li, M., Zhao, C., Li, K., Peng, M., Qin, A., Cheng, X., 2014b. Overview of trace metals in the urban soil of 31 metropolises in China. J. Geochem. Explor. 139, 31–52.
Cheng, H.X., Li, K., Li, M., Yang, K., Liu, F., Cheng, X.M., 2014c. Geochemical background and baseline value of chemical elements in urban soil in China. Earth Sci. Front. 21, 265–306 (In Chinese with English abstract).
Cheng, Z., Xie, X., Yao, W., Feng, J., Zhang, Q., Fang, J., 2014d. Multi-element geochemical mapping in Southern China. J. Geochem. Explor. 139, 183–192.
Chiu, Y.P., Li, D.W., Shiau, Y.C., 2016. Study on heavy metal characteristics of soil in phosphorus tail. J. Residuals Sci. Technol. 2, 40–50.
Cicchella, D., De, V.B., Lima, A., Albanese, S., Mc, G.R.A.R., Parrish, R.R., 2008. Heavy metal pollution and Pb isotopes in urban soils of Napoli, Italy. Geochem. Explor. Environ. Anal. 8, 103–112.
Cox, S.F., Rollinson, G., McKinley, J.M., 2017. Mineralogical characterisation to improve understanding of oral bioaccessibility of Cr and Ni in basaltic soils in Northern Ireland. J. Geochem. Explor. 183, 166–177.
Dong, M., Dong, G., Mo, X., Santosh, M., Zhu, D., Yu, J., Nie, F., Hu, Z., 2013. Geochemistry, zircon U–Pb geochronology and Hf isotopes of granites in the baoshan block, western yunnan: implications for early paleozoic evolution along the gondwana margin. Lithos 179, 36–47.
Egozcue, J.J., Pawlowsky-Glahn, V., Mateu-Figueras, G., Barceló-Vidal, C., 2003. Isometric logratio transformations for compositional data analysis. Math. Geol. 35, 279–300.
Ettler, V., 2016. Soil contamination near non-ferrous metal smelters: a review. Appl. Geochem. 64, 56–74.
Feng, H., Jiang, H., Gao, W., Weinstein, M.P., Zhang, Q., Zhang, W., Yu, L., Yuan, D., Tao, J., 2011. Metal contamination in sediments of the western Bohai Bay and adjacent estuaries. China 92, 1185–1197.
Ghrefat, H.A., Abu-Rukah, Y., Rosen, M.A., 2011. Application of geoaccumulation index and enrichment factor for assessing metal contamination in the sediments of Kafrain Dam, Jordan. Environ. Monit. Assess. 178, 95–109.
Goldhaber, M.B., Morrison, J.M., Holloway, J.M., Wanty, R.B., Helsel, D.R., Smith, D.B., 2009. A regional soil and sediment geochemical study in northern California. Appl. Geochem. 24, 1482–1499.
Gong, C., Ma, L., Cheng, H., Liu, Y., Xu, D., Li, B., Liu, F., Ren, Y., Liu, Z., Zhao, C., Yang, K., Nie, H., Lang, C., 2014. Characterization of the particle size fraction associated heavy metals in tropical arable soils from Hainan Island, China. J. Geochem. Explor. 139, 109–114.
Hamon, R.E., McLaughlin, M.J., Gilkes, R.J., Rate, A.W., Zarcinas, B., Robertson, A., Cozens, G., Radford, N., Bettenay, L., 2004. Geochemical indices allow estimation of heavy metal background concentrations in soils. Global Biogeochem. Cycles 18, 1–6.
Hamzeh, M.A., Aftabi, A., Mirzaee, M., 2011. Assessing geochemical influence of traffic and other vehicle-related activities on heavy metal contamination in urban soils of Kerman city, using a GIS-based approach. Environ. Geochem. Health 33, 577–594.
Jackson, C.E., McKinley, J.M., Ofterdinger, U., Fogarty, D., Atkinson, P.M., Palmer, S., 2016. Investigating relations between environmental toxins in Northern Irish soils and streams and Chronic Kidney Disease prevalence. Appl. Geochem. 75, 236–246.
Kelepertzis, E., Galanos, E., Mitsis, I., 2013. Origin, mineral speciation and geochemical baseline mapping of Ni and Cr in agricultural topsoils of Thiva Valley (central Greece). J. Geochem. Explor. 125, 56–68.
Kuo, S., Heilman, P.E., Baker, A.S., 1983. Distribution and forms of copper, zinc, cadmium, iron, and manganese in soils near a copper smelter. Soil Sci. 135, 101–109.
Leifeld, J., Bassin, S., Fuhrer, J., 2005. Carbon stocks in Swiss agricultural soils predicted by land-use, soil characteristics, and altitude. Agric. Ecosyst. Environ. 105, 255–266.
Li, X.H., Cheng, H.X., Zhao, C.D., Xu, X.B., 2010. Mercury contamination in the topsoil and subsoil of urban areas of Beijing, China. Bull. Environ. Contam. Toxicol. 85, 224–228.
Li, Z., Ma, Z., van der Kuijp, T.J., Yuan, Z., Huang, L., 2014a. A review of soil heavy metal pollution from mines in China: pollution and health risk assessment. Sci. Total Environ. 468–469, 843–853.
Li, M., Xi, X., Xiao, G., Cheng, H., Yang, Z., Zhou, G., Ye, J., Li, Z., 2014b. National multi-purpose regional geochemical survey in China. J. Geochem. Explor. 139, 21–30.
Li, D., Chen, Y., Hou, K., Lu, Z., Cui, D., 2015. Detrital zircon record of Paleozoic and Mesozoic meta-sedimentary strata in the eastern part of the Baoshan block: implications of their provenance and the tectonic evolution of the southeastern margin of the Tibetan plateau. Lithos 227, 194–204.
Liénard, A., Brostaux, Y., Colinet, G., 2014. Soil contamination near a former Zn–Pb ore-treatment plant: evaluation of deterministic factors and spatial structures at the landscape scale. J. Geochem. Explor. 147, 107–116.
Loska, K., Wiechula, D., Barska, B., Cebula, E., Chojnecka, A., 2003. Assessment of arsenic enrichment of cultivated soils in Southern Poland. Pol. J. Environ. Stud. 12, 187–192.
Luo, X.S., Yu, S., Zhu, Y.G., Li, X.D., 2012. Trace metal contamination in urban soils of China. Sci. Total Environ. 421–422, 17–30.
McGrath, D., Tunney, H., 2010. Accumulation of cadmium, fluorine, magnesium, and zinc in soil after application of phosphate fertilizer for 31 years in a grazing trial. J. Plant Nutr. Soil Sci. 173, 548–553.
Ministry of Ecology and Environment of The People's Republic of China, 2018. Soil environmental quality-Risk control for soil contamination of agricultural land (GB-15618-2018). In: Ministry of Ecology and Environment of the People's Republic of China. Beijing. (In Chinese).
Ministry of Land and Resources of the People's Republic of China, 2014. Code of Geochemical Rock Survey of China (DZ/T 0248-2014) (In Chinese).
Müller, G., 1969. Index of geoaccumulation in sediments of the rhine river. J. Geol. 2, 108–118.
Nannoni, F., Protano, G., Riccobono, F., 2011. Fractionation and geochemical mobility of heavy elements in soils of a mining area in northern Kosovo. Geoderma 161, 63–73.
Odewande, A.A., Abimbola, A.F., 2008. Contamination indices and heavy metal concentrations in urban soil of Ibadan metropolis, southwestern Nigeria. Environ. Geochem. Health 30, 243–254.
Palmer, S., Cox, S.F., McKinley, J.M., Ofterdinger, U., 2014. Soil-geochemical factors controlling the distribution and oral bioaccessibility of nickel, vanadium and chromium in soil. Appl. Geochem. 51, 255–267.
Pawlowsky-Glahn, V., Buccianti, A., 2011. Compositional Data Analysis: Theory and Applications. John Wiley & Sons.
Pawlowsky-Glahn, V., Egozcue, J.J., 2001. Geometric approach to statistical analysis on the simplex. Stoch. Environ. Res. Risk Assess. 15, 384–398.
Pinto, M.M.S.C., Silva, M.M., Neiva, A.M.R., 2004. Pollution of water and stream sediments associated with the vale de abrutiga uranium mine, Central Portugal. Mine Water Environ. 23, 66–75.
Poňavič, M., Wittlingerová, Z., Čoupek, P., Buda, J., 2018. Soil geochemical mapping of the central part of Prague, Czech Republic. J. Geochem. Explor. 187, 118–130.
Prathumratana, L., Kim, R., Kim, K.W., 2018. Lead contamination of the mining and smelting district in Mitrovica, Kosovo. Environ. Geochem. Health 1–12.
Purswani, E., Pathak, B., 2018. Assessment of soil characteristics in different land-use systems in Gandhinagar, Gujarat. Proceedings of the International Academy of Ecology and Environmental Sciences 8 (3), 162–171.
Rate, A.W., 2018. Multielement geochemistry identifies the spatial pattern of soil and sediment contamination in an urban parkland, Western Australia. Sci. Total Environ. 627, 1106–1120.
Reimann, C., Caritat, P. de, 2000. Intrinsic flaws of element enrichment factors (EFs) in environmental geochemistry. Environ. Sci. Technol. 34, 5084–5091.
Reimann, C., Caritat, P. de, 2005. Distinguishing between natural and anthropogenic sources for elements in the environment: regional geochemical surveys versus enrichment factors. Sci. Total Environ. 337, 91–107.
Rudnick, R.L., Gao, S., 2003. Composition of the continental crust. In: Rudnick, R.L. (Ed.), The Crust. Elsevier-Pergamon, Oxford, pp. 1–64.
Ryan, J.D., Windom, H.L., 1988. A Geochemical and Statistical Approach for Assessing Metal Pollution in Coastal Sediments. Springer Berlin Heidelberg, pp. 47–58.
Sinex, S.A., Wright, D.A., 1988. Distribution of trace metals in the sediments and biota of Chesapake Bay. Mar. Pollut. Bull. 19, 425–431.
Sucharova, J., Suchara, I., Hola, M., Marikova, S., Reimann, C., Boyd, R., Filzmoser, P., Englmaier, P., 2012. Top/bottom-soil ratios and enrichment factors: what do they really show? Appl. Geochem. 27, 138–145.
Tashakor, M., Zuhairi, W.Y.W., Mohamad, H., Ghani, A.A., 2014. Geochemical characteristics of serpentinite soils from Malaysia. Malaysian Journal of Soil Science 18, 35–49.
Thio-Henestrosa, S., Martin-Fernandez, J.A., 2006. Detailed guide to CoDaPack: a freeware compositional software. Geological Society London Special Publications 264, 101–118.
Thiombane, M., Di Bonito, M., Albanese, S., Zuzolo, D., Lima, A., De Vivo, B., 2019. Geogenic versus anthropogenic behaviour and geochemical footprint of Al, Na, K and P in the Campania region (Southern Italy) soils through compositional data analysis and enrichment factor. Geoderma 335, 12–26.
Tolosana-Delgado, R., McKinley, J., 2016. Exploring the joint compositional variability of major components and trace elements in the Tellus soil geochemistry survey (Northern Ireland). Appl. Geochem. 75, 263–276.

Wang, Y., Zhang, A., Fan, W., Peng, T., Zhang, F., Zhang, Y., Bi, X., 2010. Petrogenesis of late Triassic post-collisional basaltic rocks of the Lancangjiang tectonic zone, southwest China, and tectonic implications for the evolution of the eastern Paleotethys: geochronological and geochemical constraints. Lithos 120, 529–546.

Wang, Y., Xing, X., Cawood, P.A., Lai, S., Xia, X., Fan, W., Liu, H., Zhang, F., 2013. Petrogenesis of early Paleozoic peraluminous granite in the Sibumasu Block of SW Yunnan and diachronous accretionary orogenesis along the northern margin of Gondwana. Lithos 182–183, 67–85.

Wang, X., Liu, X., Han, Z., Zhou, J., Xu, S., Zhang, Q., Chen, H., Bo, W., Xia, X., 2015. Concentration and distribution of mercury in drainage catchment sediment and alluvial soil of China. J. Geochem. Explor. 154, 32–48.

Wang, X.Q., Zhou, J., Xu, S.F., Chi, Q.H., Nie, L.S., ZhangB, M., Yao, W.S., Wang, Wei, Liu, H.L., Liu, D.S., Han, Z.X., Liu, Q.Q., 2016. China soil geochemical baselines networks: data characteristics. Chin. Geol. 43 (5), 1469–1480 (in Chinese with English abstract).

Wiesmeier, M., Hübner, R., Barthold, F., Spörlein, P., Geuß, U., Hangen, E., Reischl, A., Schilling, B., von Lützow, M., Kögel-Knabner, I., 2013. Amount, distribution and driving factors of soil organic carbon and nitrogen in cropland and grassland soils of southeast Germany (Bavaria). Agric. Ecosyst. Environ. 176, 39–52.

Zhang, J., Liu, C.L., 2001. Riverine composition and estuarine geochemistry of particulate metals in China-weathering features, anthropogenic impact and chemical fluxes. Estuar. Coast Shelf Sci. 54, 1051–1070.

Zhang, X.P., Wei, D., Yang, X.M., 2002. The background concentrations of 13 soil trace elements and their relationships to parent materials and vegetation in Xizang (Tibet), China. J. Asian Earth Sci. 21, 167–174.

Zhang, H., Luo, Y., Makino, T., Wu, L., Nanzyo, M., 2013. The heavy metal partition in size-fractions of the fine particles in agricultural soils contaminated by waste water and smelter dust. J. Hazard Mater. 248–249, 303–312.

Zhang, H., Chen, J., Li, Z., Yang, G., Li, D., 2014. Anthropogenic mercury enrichment factors and contributions in soils of Guangdong Province, South China. J. Geochem. Explor. 144, 312–319.

Zhang, J., Li, H., Zhou, Y., Dou, L., Cai, L., Mo, L., You, J., 2018. Bioavailability and soil-to-crop transfer of heavy metals in farmland soils: a case study in the Pearl River Delta, South China. Environ. Pollut. 235, 710–719.

Zhang, L., McKinley, M.J., Cooper, M., Peng, M., Wang, Q., Song, Y., Cheng, H., 2020. A regional soil and river sediment geochemical study in Baoshan area, Yunnan province, southwest China. J. Geochem. Explor. 217, 106557.